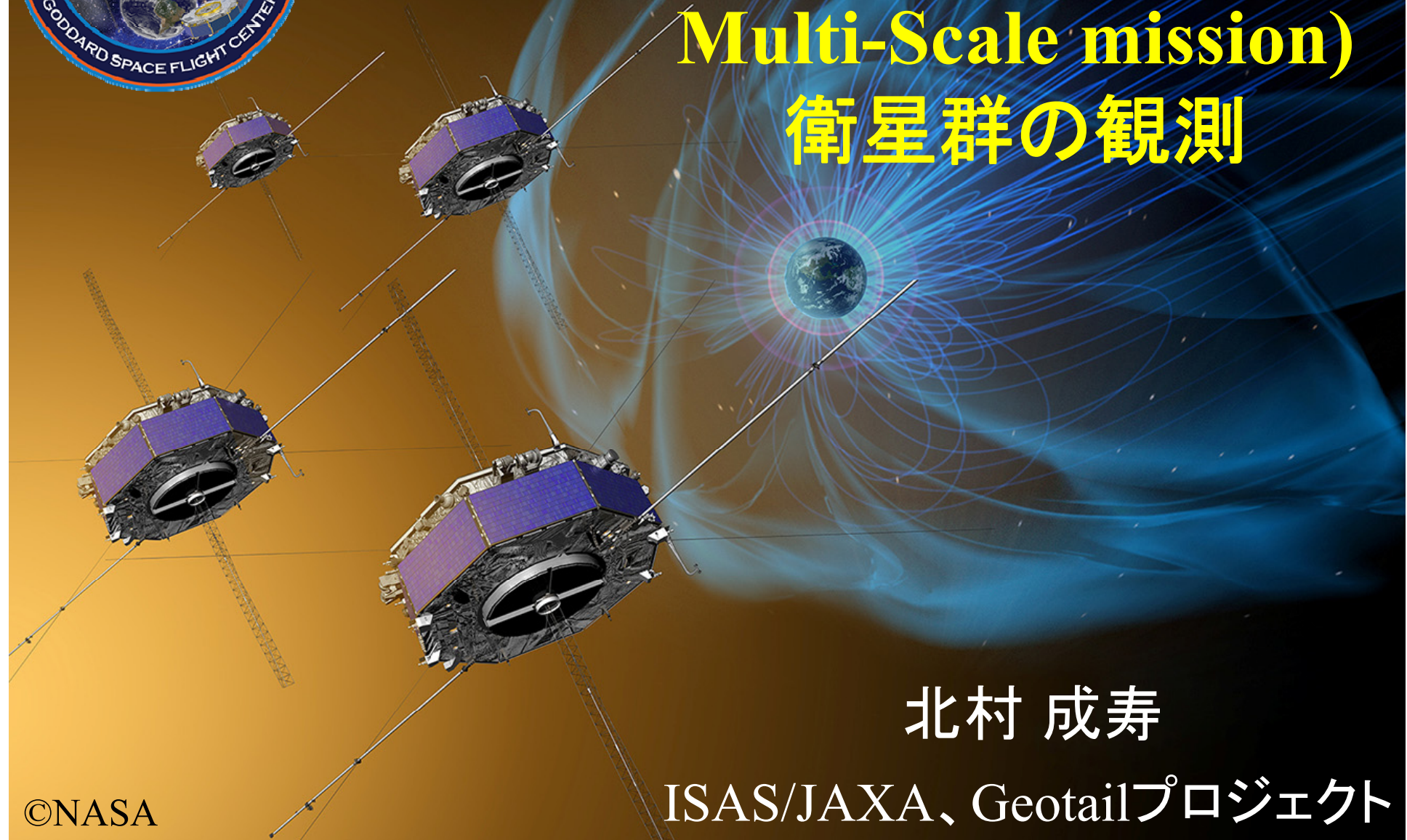




16 September 2016

MMS(Magnetospheric Multi-Scale mission) 衛星群の観測



©NASA

北村 成寿

ISAS/JAXA、Geotailプロジェクト

Contents

1. MMS衛星群の観測目標、領域
2. MMS衛星群の観測機器



<http://mms.gsfc.nasa.gov/>

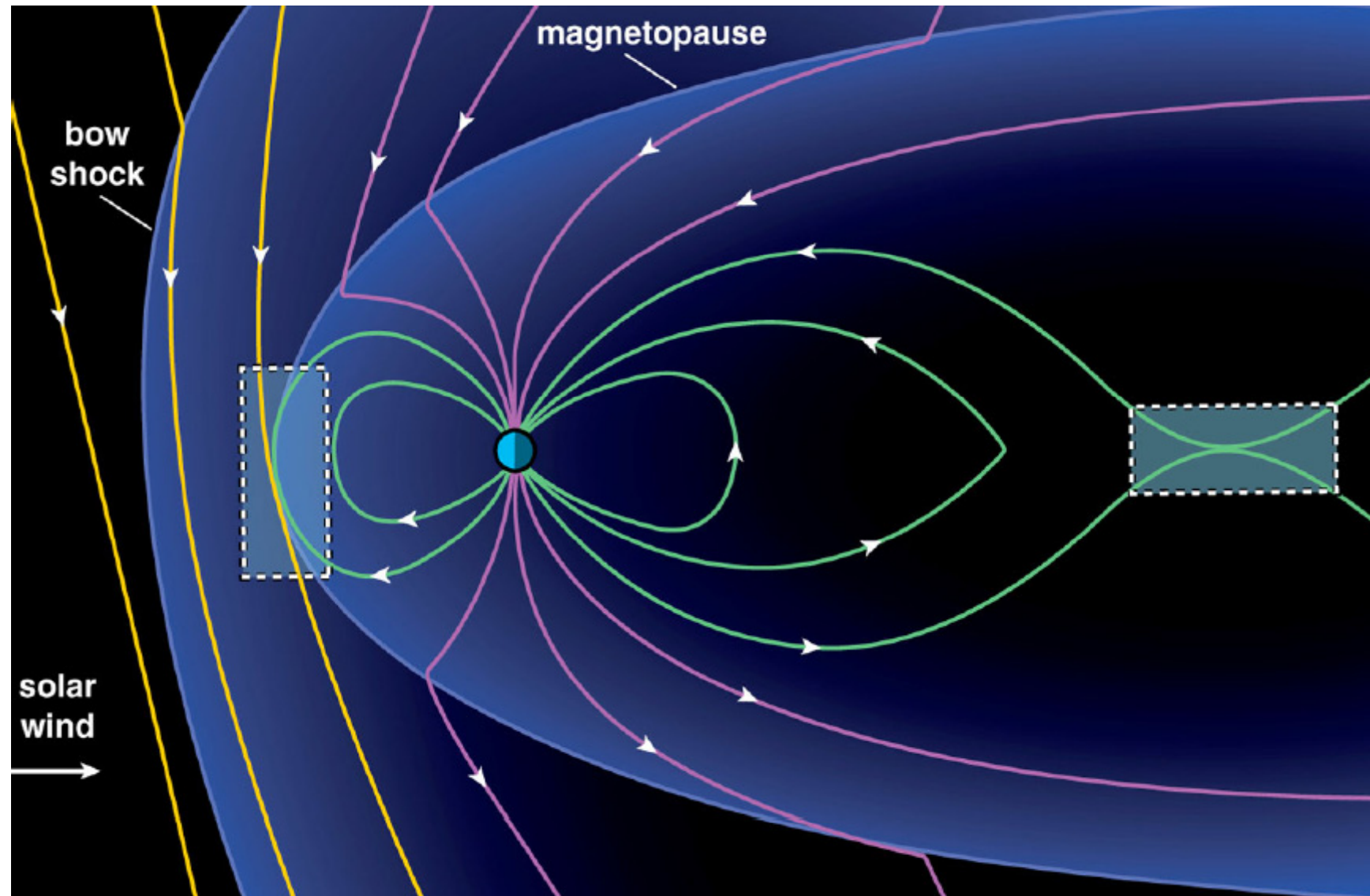
Launched on March 12 (日本時間13日), 2015
初期遠地点: ~0300 MLT



<http://mms.gsfc.nasa.gov/>

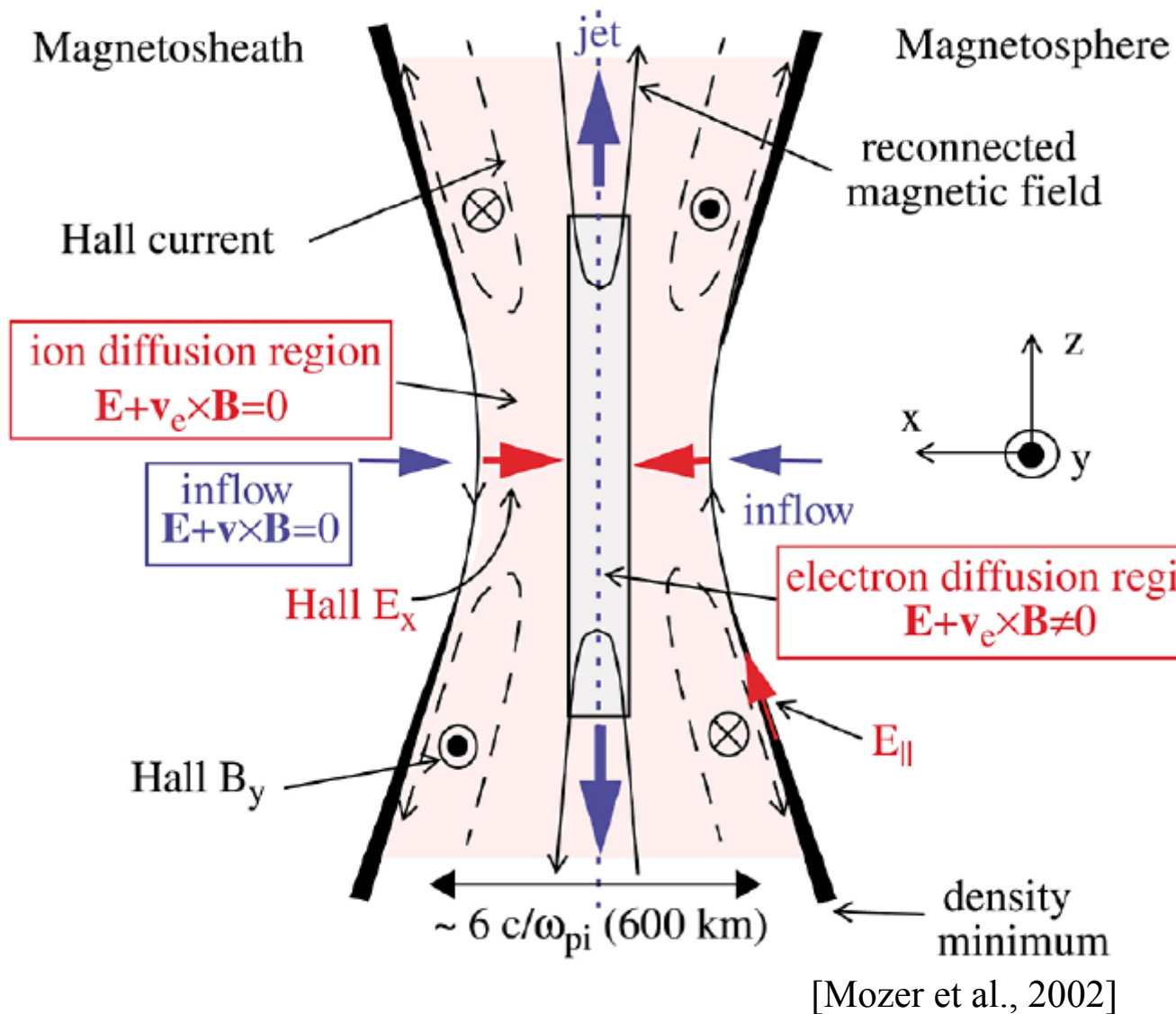
1. MMS衛星群の観測目標、領域

◆観測対象(リコネクション)



[Burch et al., 2016]

◆リコネクションの電子拡散領域



Electron diffusion region
Thickness: 1–30 km?
Width: <10–300 km?
[Fuselier et al., 2016]

Electron diffusion region
での滞在時間: ~0.1 sec
(幅~5 km、移動速度~50
km/sを仮定)
[Burch et al., 2016]
(THEMISの粒子観測の
時間分解能: 3 sec)

◆姿勢、衛星間距離

Electron diffusion region

Thickness: 1–30 km?

Width: <10–300 km?

[Fuselier et al., 2016]

衛星間距離(4機編隊、三角錐)

10–160 km (Dayside, $\sim 12 R_E$)

10?–160 km (Magnetotail, $\sim 25 R_E$)

※内部磁気圏付近では間隔が広がり
三角錐の形状も乱れる

ジャイロ半径(磁場強度: 40 nT)

H^+ : 35 km (100 eV), 115 km (1 keV)

電子: 0.84 km (100 eV), 2.7 km (1 keV)

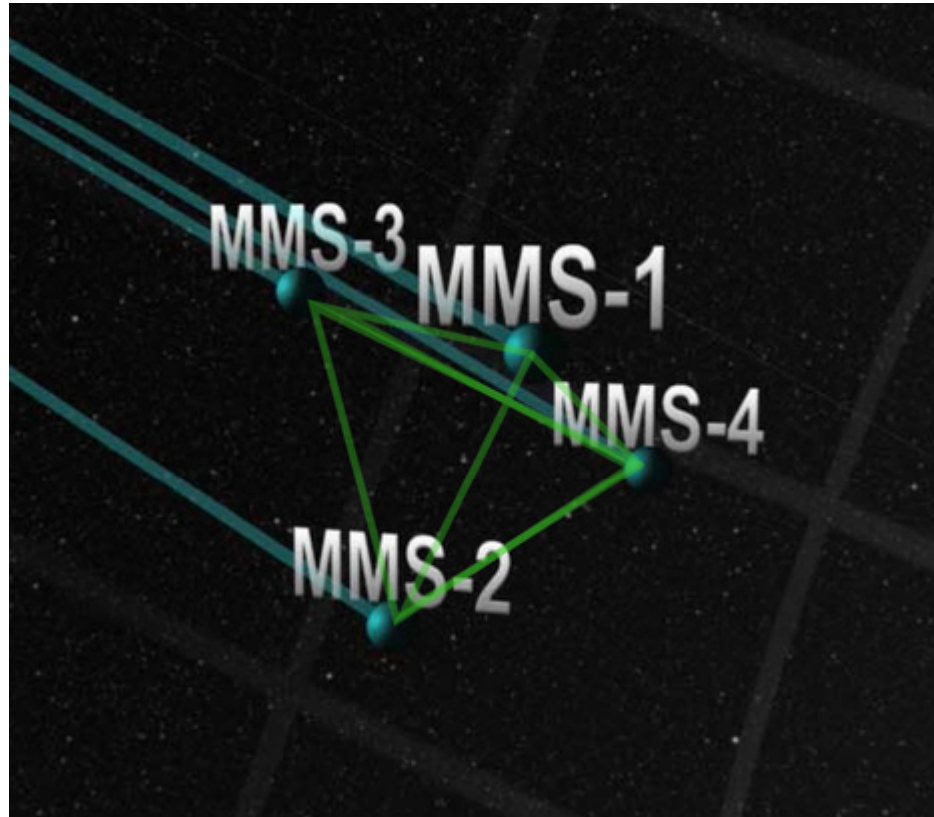
スピン周期

~20 sec (~3 rpm, ~0.05 Hz)

スピン軸

黄道面に垂直からわずかに傾斜(<5°)

※電場プローブが衛星本体の日陰に入る事を避ける



<http://www.nasa.gov/feature/goddard/nasas-mms-spacecraft-achieve-tightest-flying-formation-ever>

Commission (Phase 0):

March 12, 2015–August 31, 2015

(磁場のLevel-2データが作成されていない
(公開データ無し)ため、チーム外ではデータ
の解析は難しい)

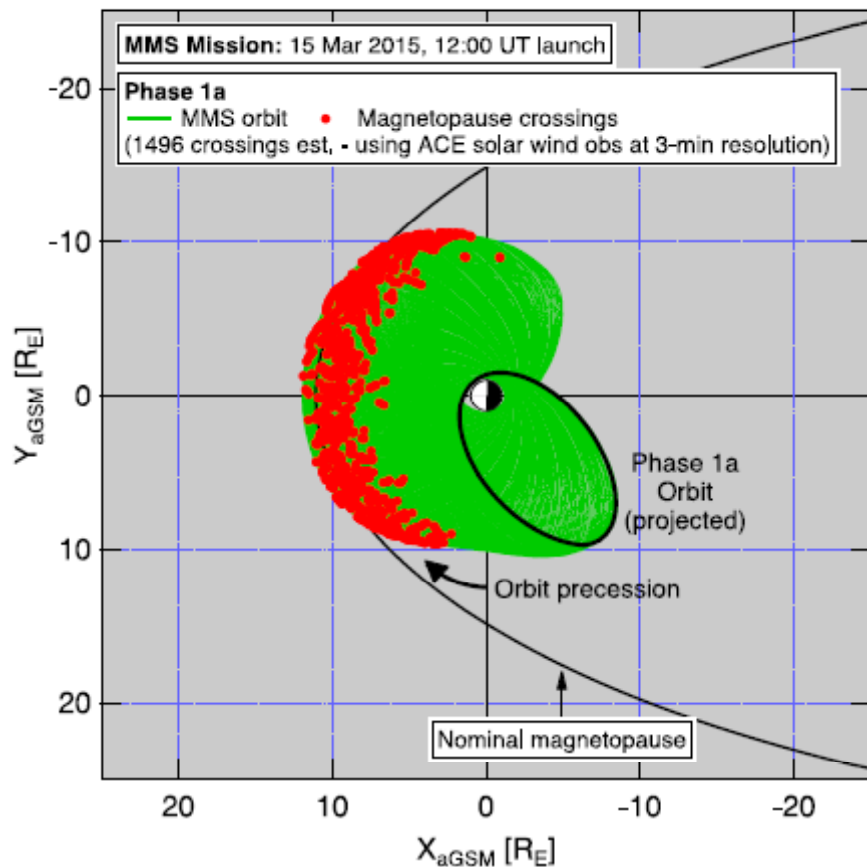
◆軌道、Region Of Interest (ROI)

■Phase 1a (Magnetopause reconnection 1)

(September 1, 2015–March 7, 2016)

遠地点: $12 R_E$, 1800–0600 MLT

軌道傾斜角: 28° 周期: ~ 23 h 54 min



衛星間距離

160 km: July 9, 2015 (2 weeks after the beginning of Phase 1a)

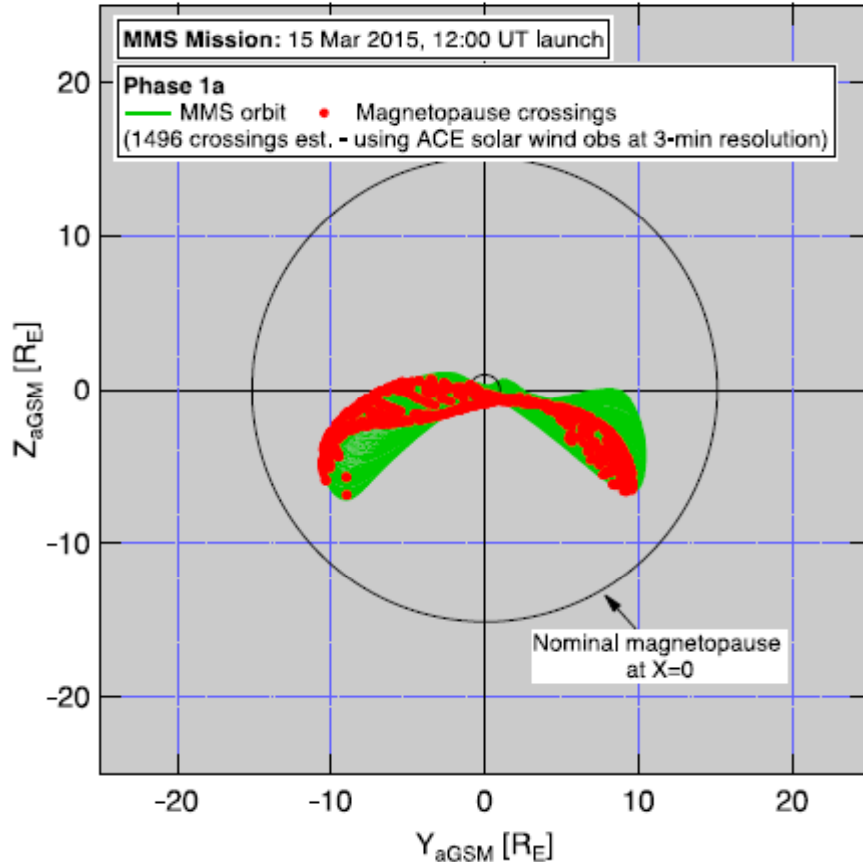
60 km: September 17, 2015 (2 weeks)

25 km: October 1, 2015 (2 weeks)

10 km: October 15, 2015 (9 weeks)

40 km: December 17, 2015 (4 weeks)

10 km: January 14, 2016 (7 weeks)



[Fuselier et al., 2016]

◆軌道、Region Of Interest (ROI)

■Phase 1a (Magnetopause reconnection 1)

(September 1, 2015–March 7, 2016)

遠地点: $12 R_E$, 1800–0600 MLT

軌道傾斜角: 28° 周期: ~ 23 h 54 min

Near Van Allen Probes (apogee in MLT)

Sometimes near Geotail around the MMS apogee

衛星間距離

7

160 km: July 9, 2015 (2 weeks after the beginning of Phase 1a)

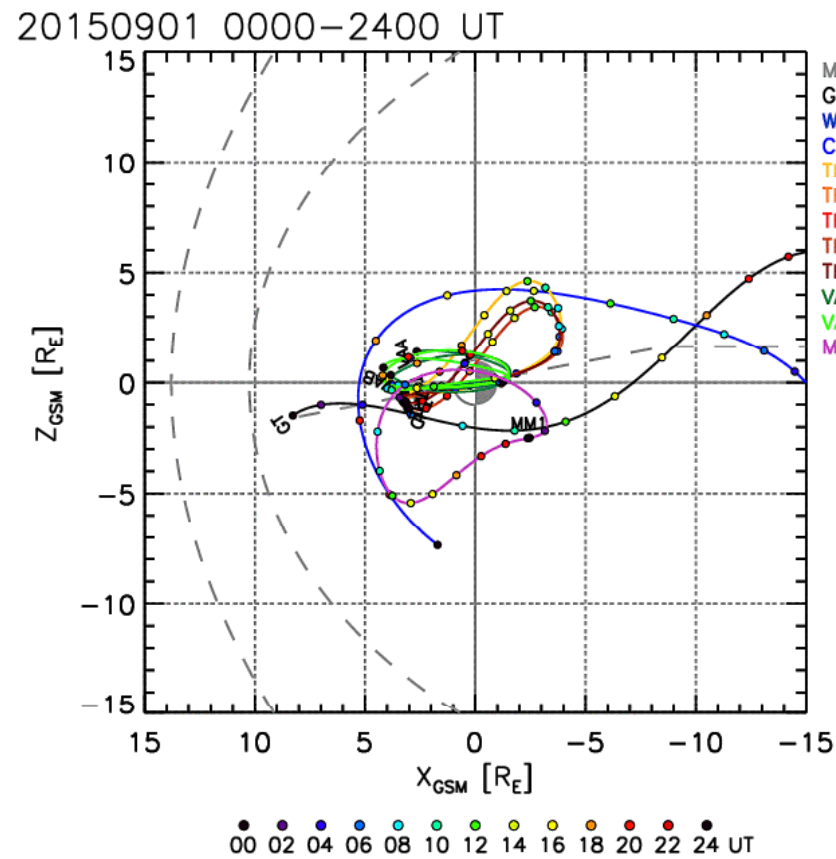
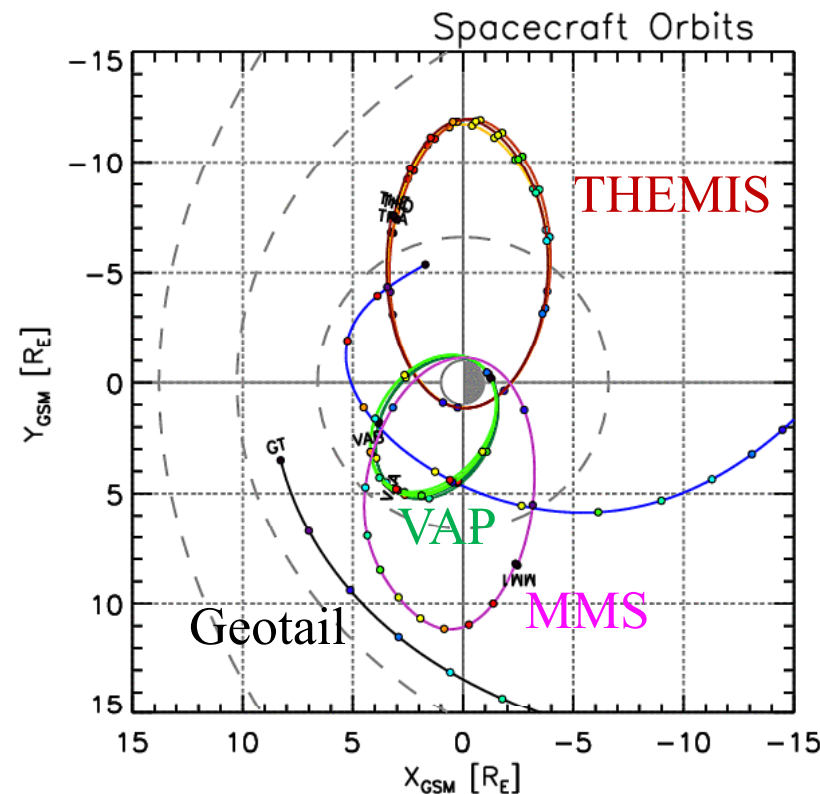
60 km: September 17, 2015 (2 weeks)

25 km: October 1, 2015 (2 weeks)

10 km: October 15, 2015 (9 weeks)

40 km: December 17, 2015 (4 weeks)

10 km: January 14, 2016 (7 weeks)



◆軌道、Region Of Interest (ROI)

■Phase 1a (Magnetopause reconnection 1)

(September 1, 2015–March 7, 2016)

遠地点: $12 R_E$, 1800–0600 MLT

軌道傾斜角: 28° 周期: ~ 23 h 54 min

Near Van Allen Probes (apogee in MLT)

Sometimes near Geotail around the MMS apogee

衛星間距離

160 km: July 9, 2015 (2 weeks after the beginning of Phase 1a)

60 km: September 17, 2015 (2 weeks)

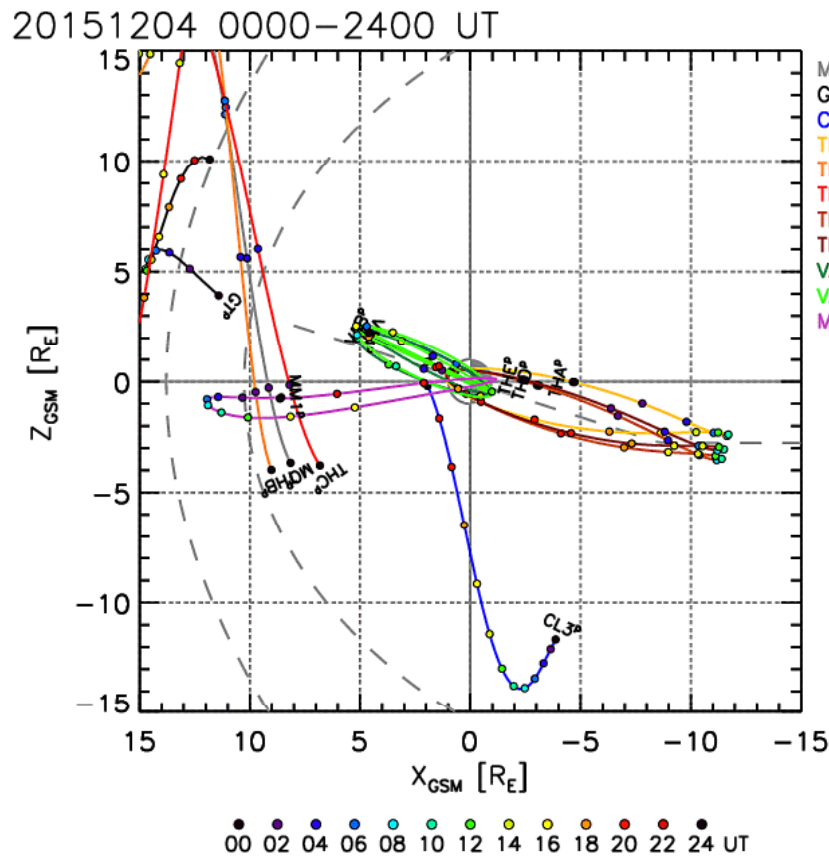
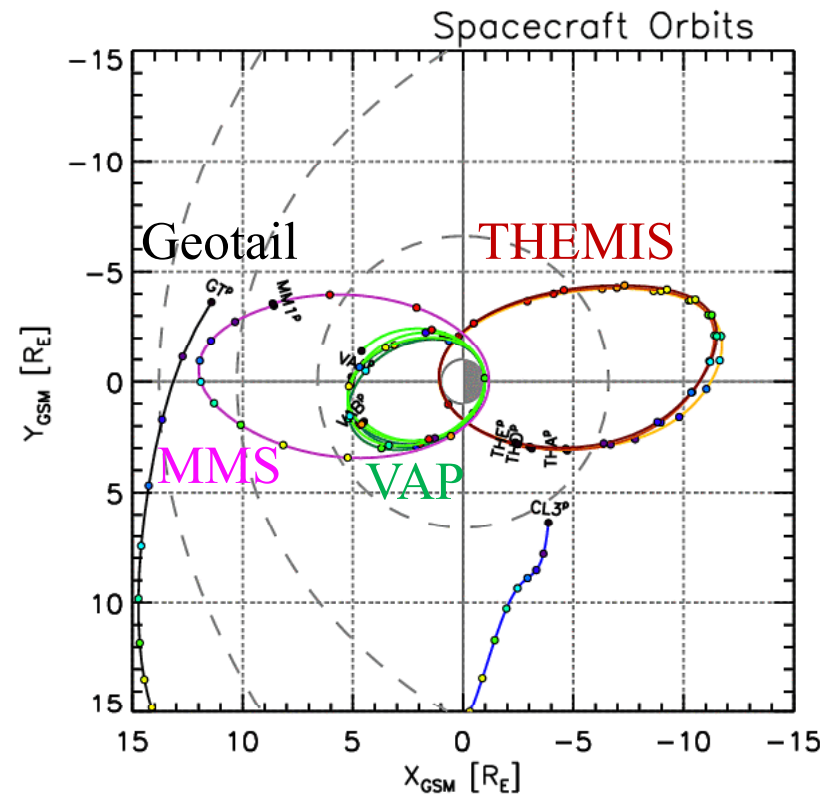
25 km: October 1, 2015 (2 weeks)

10 km: October 15, 2015 (9 weeks)

40 km: December 17, 2015 (4 weeks)

10 km: January 14, 2016 (7 weeks)

8



◆軌道、Region Of Interest (ROI)

■Phase 1a (Magnetopause reconnection 1)

(September 1, 2015–March 7, 2016)

遠地点: $12 R_E$, 1800–0600 MLT

軌道傾斜角: 28° 周期: ~ 23 h 54 min

Near Van Allen Probes (apogee in MLT)

Sometimes near Geotail around the MMS apogee

衛星間距離

160 km: July 9, 2015 (2 weeks after the beginning of Phase 1a)

60 km: September 17, 2015 (2 weeks)

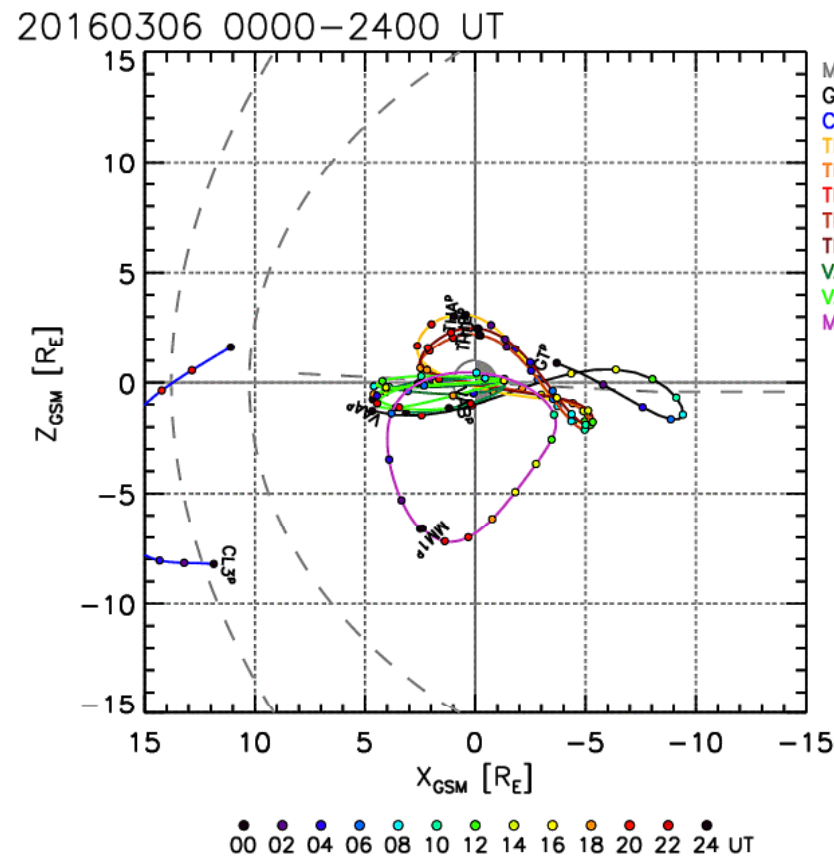
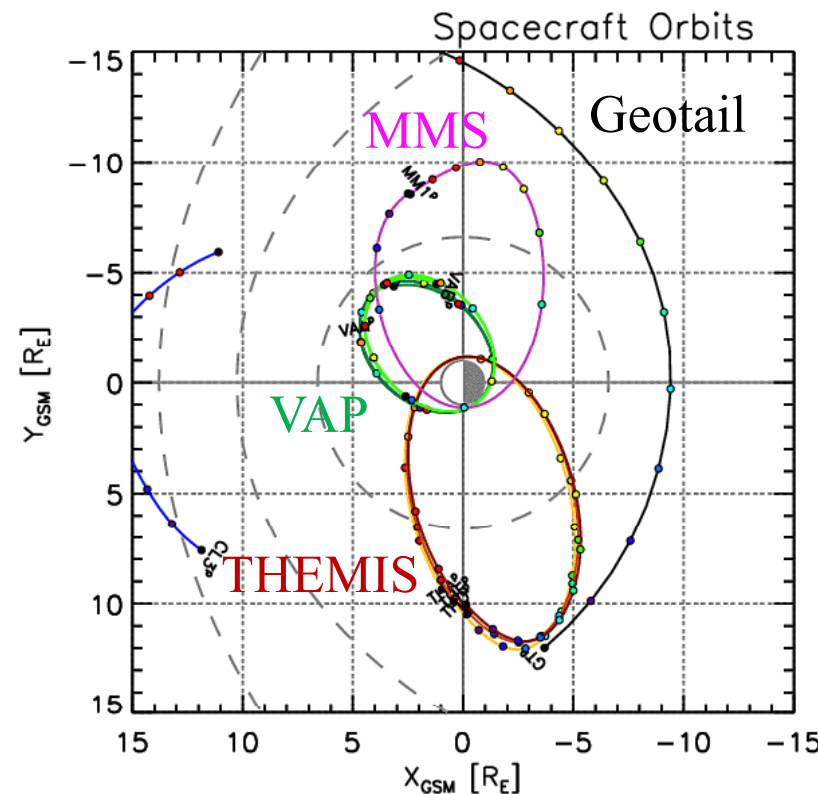
25 km: October 1, 2015 (2 weeks)

10 km: October 15, 2015 (9 weeks)

40 km: December 17, 2015 (4 weeks)

10 km: January 14, 2016 (7 weeks)

9



◆軌道、Region Of Interest (ROI)

10

■Phase 1x (Transition to Phase 1b)

(March 8, 2016–September 11, 2016)

遠地点: $12 R_E$, 0600–1800 MLT

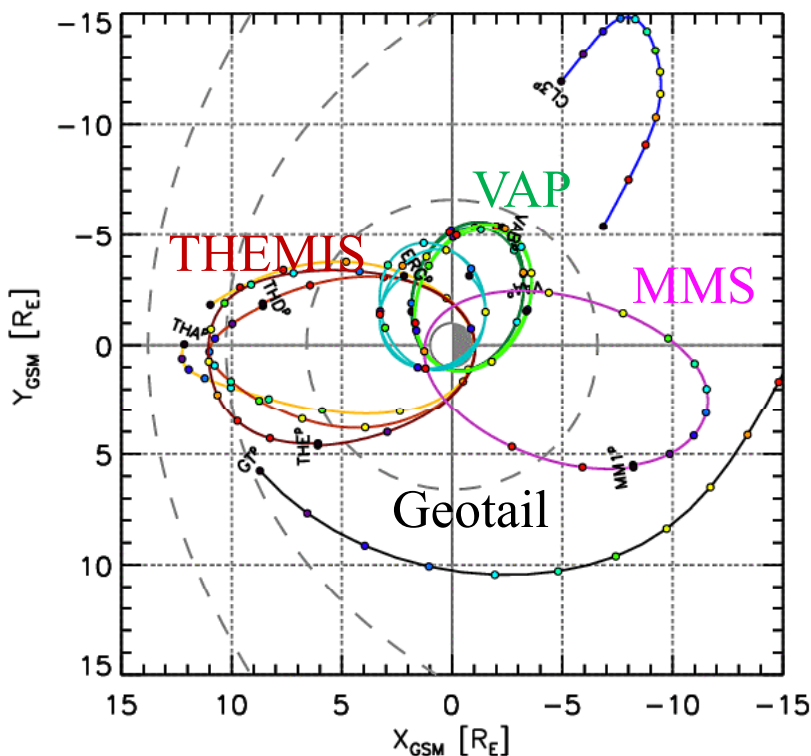
軌道傾斜角: 28° 周期: ~ 23 h 54 min

(August 9–26の一部時間(各軌道2時間))

以外では**低エネルギー**プラズマ観測はイ
オン質量分析のみ、電子なし)

(Sometimes near Geotail)

4 July, 2016

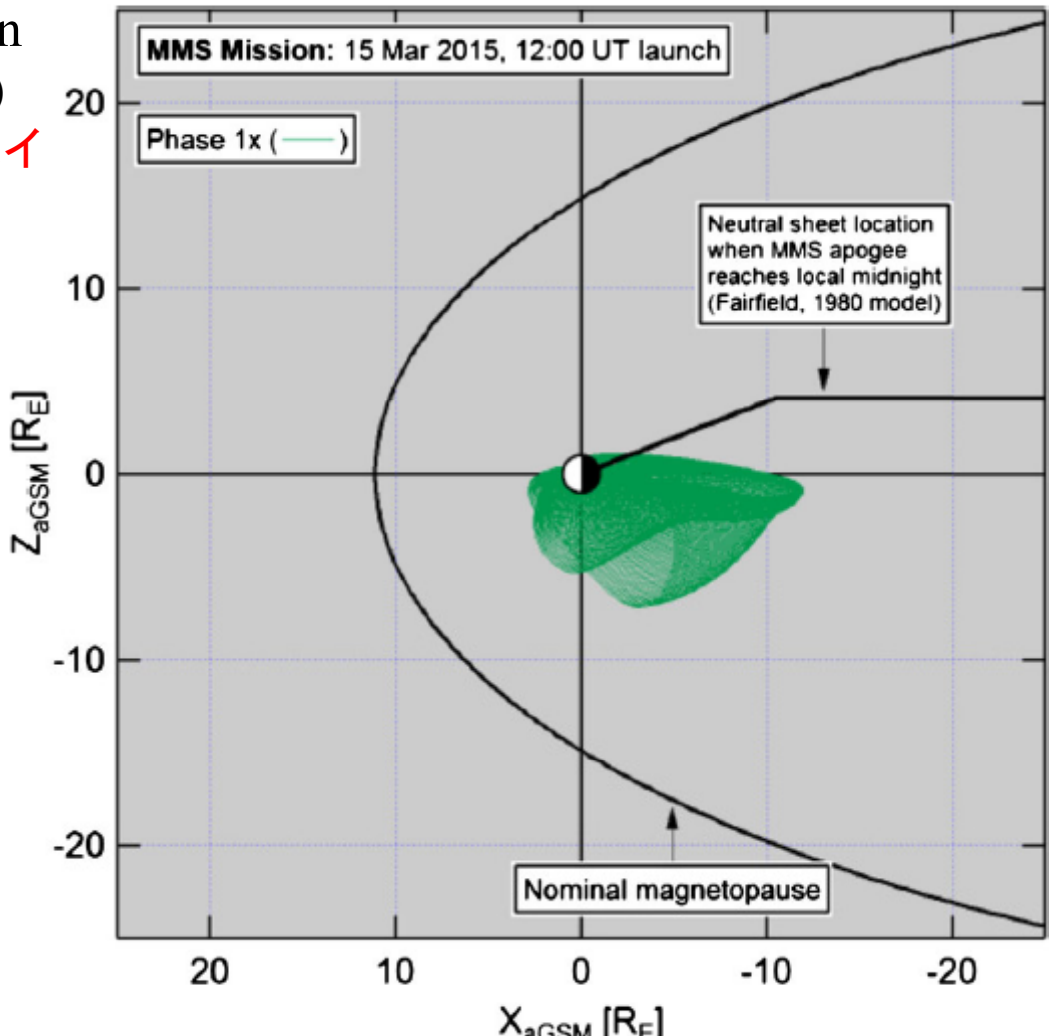


衛星間距離

10 km: January 14, 2016 (from Phase-1a)

40 km: March 24, 2016

10 km: August 31, 2016



[Fuselier et al., 2016]

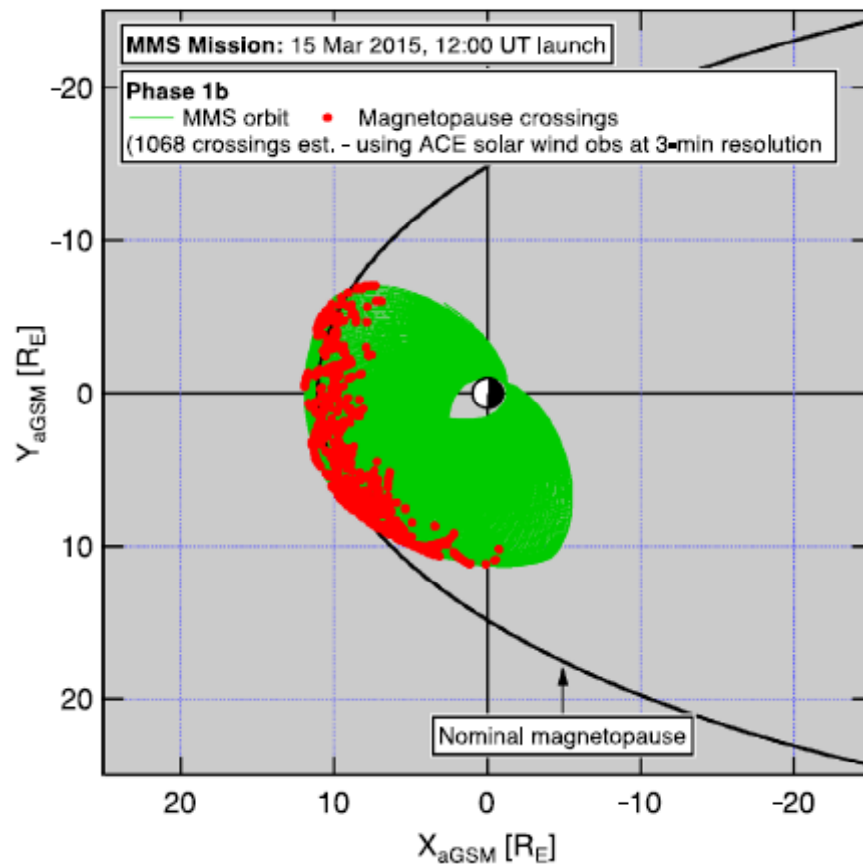
◆軌道、Region Of Interest (ROI)

■Phase 1b (Magnetopause reconnection 2)

(September 12, 2016–January 31, 2017)

遠地点: $12 R_E$, 1800–1000 MLT

軌道傾斜角: 28° 周期: ~ 23 h 54 min

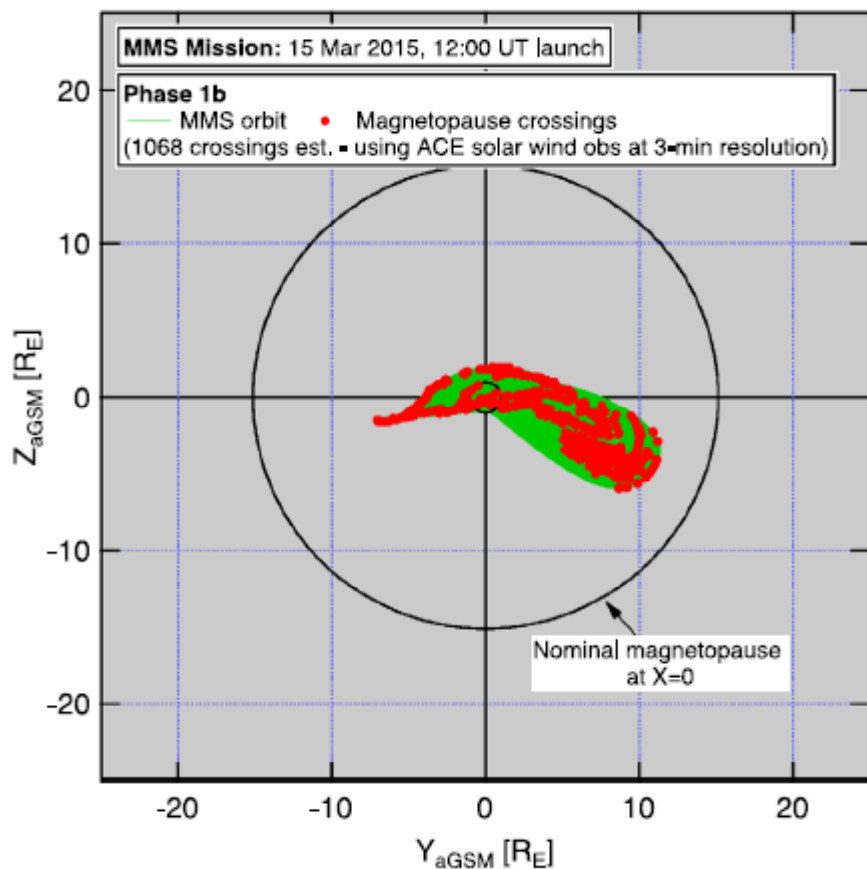


衛星間距離

10 km: August 31, 2016 (from Phase-1x)

7 km: September 21, 2016 (※予定)

Phase-1xで休みでだったFPIによる
低エネルギー plasma 観測は
September 26, 2016から再開



[Fuselier et al., 2016]

◆軌道、Region Of Interest (ROI)

12

■Phase 1b (Magnetopause reconnection 2)

(September 26, 2016–January 31, 2017)

遠地点: $12 R_E$, 1800–1000 MLT

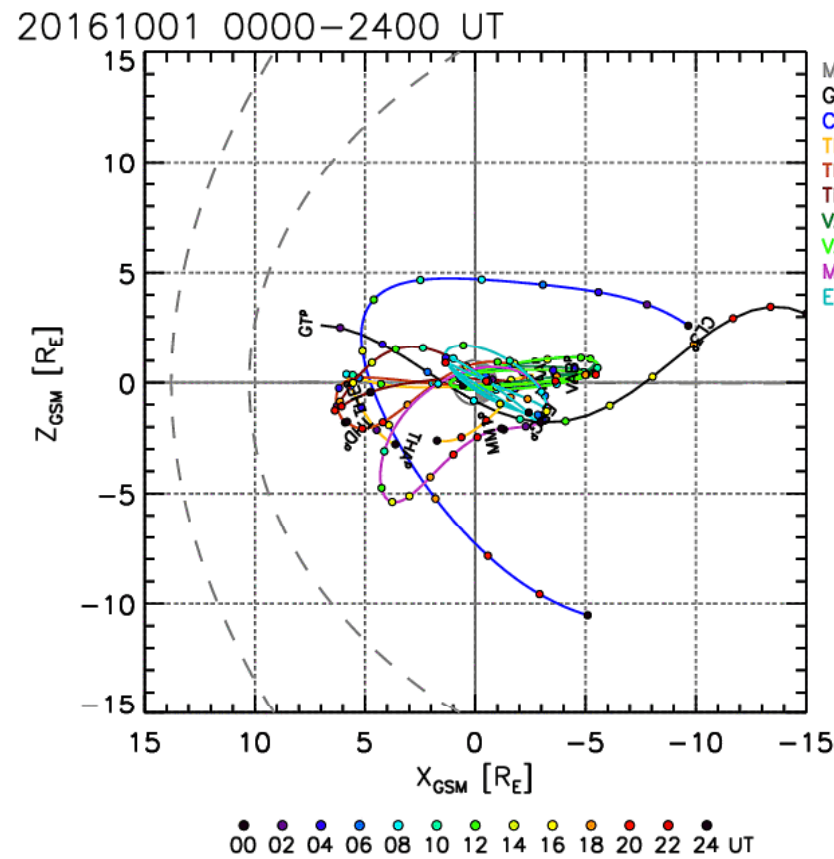
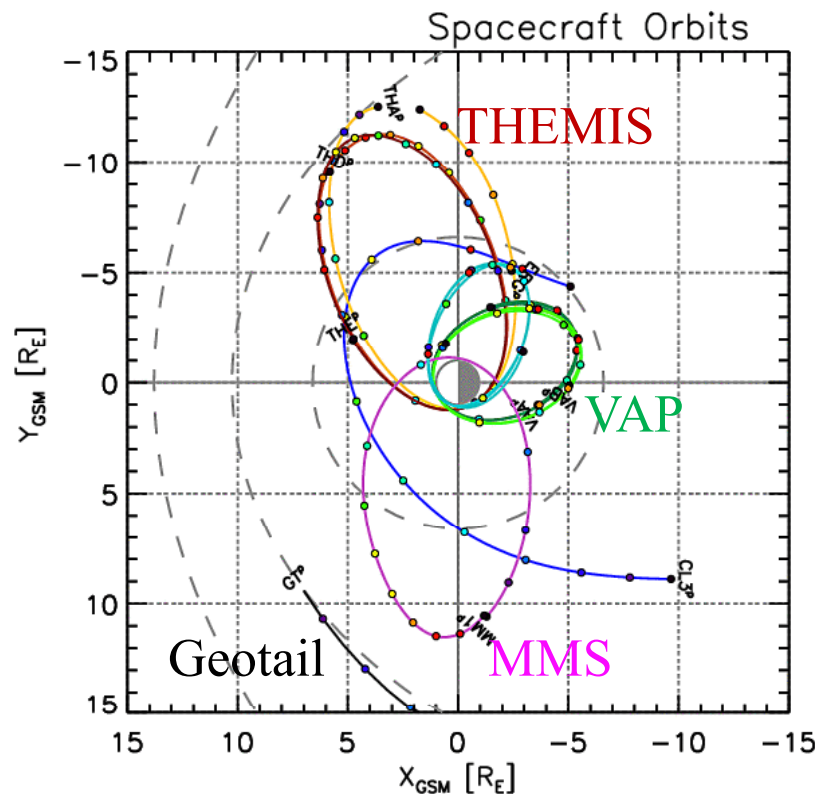
軌道傾斜角: 28° 周期: ~ 23 h 54 min

衛星間距離

10 km: August 31, 2016 (from Phase-1x)

7 km: September 21, 2016 (※予定)

Phase-1xで休みでだったFPIによる
低エネルギー plasma 観測は
September 26, 2016から再開



◆軌道、Region Of Interest (ROI)

13

■Phase 1b (Magnetopause reconnection 2)

(September 26, 2016–January 31, 2017)

遠地点: $12 R_E$, 1800–1000 MLT

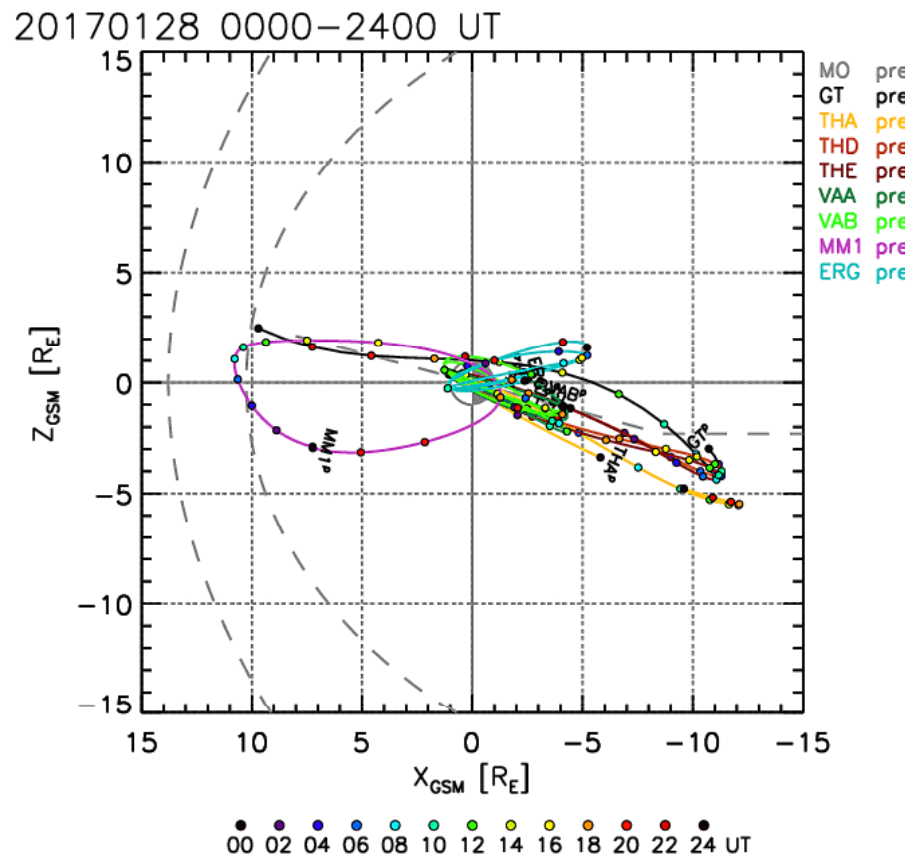
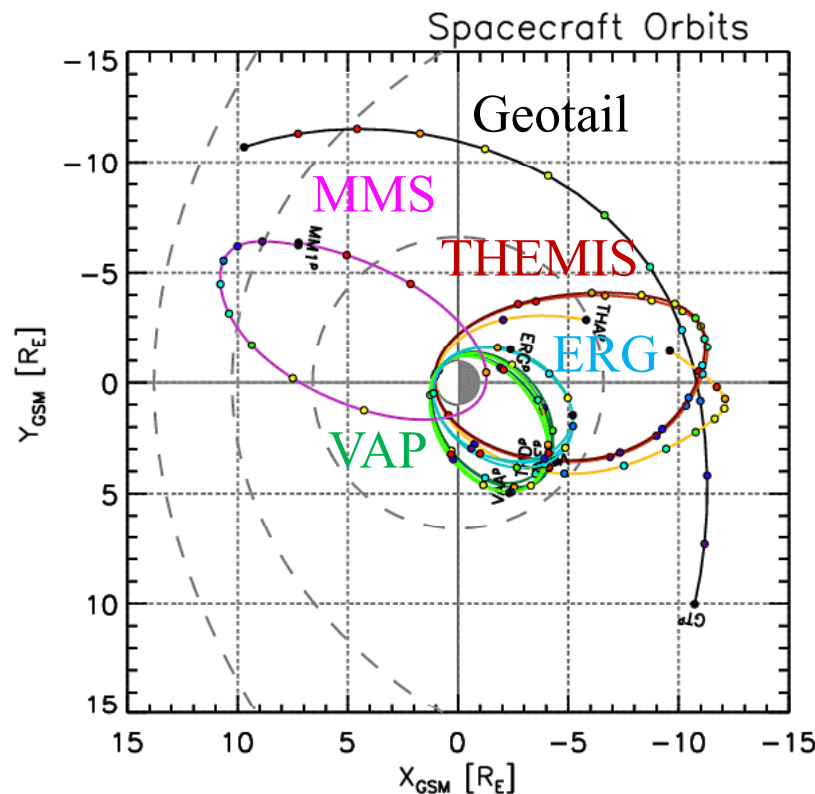
軌道傾斜角: 28° 周期: ~ 23 h 54 min

衛星間距離

10 km: August 31, 2016 (from Phase-1x)

7 km: September 21, 2016 (※予定)

Phase-1xで休みでだったFPIによる
低エネルギー plasma 観測は
September 26, 2016から再開



◆軌道、Region Of Interest (ROI)

14

■Phase 2a (Apogee raising)

(February 1, 2017–May 4, 2017)

遠地点: $12\text{--}25 R_E$, 1000–0300 MLT

Limited observations?

■Phase 2b (Magnetotail reconnection)

(May 5, 2017–August ~19, 2017)

遠地点: $25 R_E$, 0300–1800 MLT

周期: $\sim 66 \text{ h } 43 \text{ min}$

衛星間距離

10–160 km (ただし実際に<30 kmが可能かはGPSによる位置決定精度に依存)

■Extended Mission

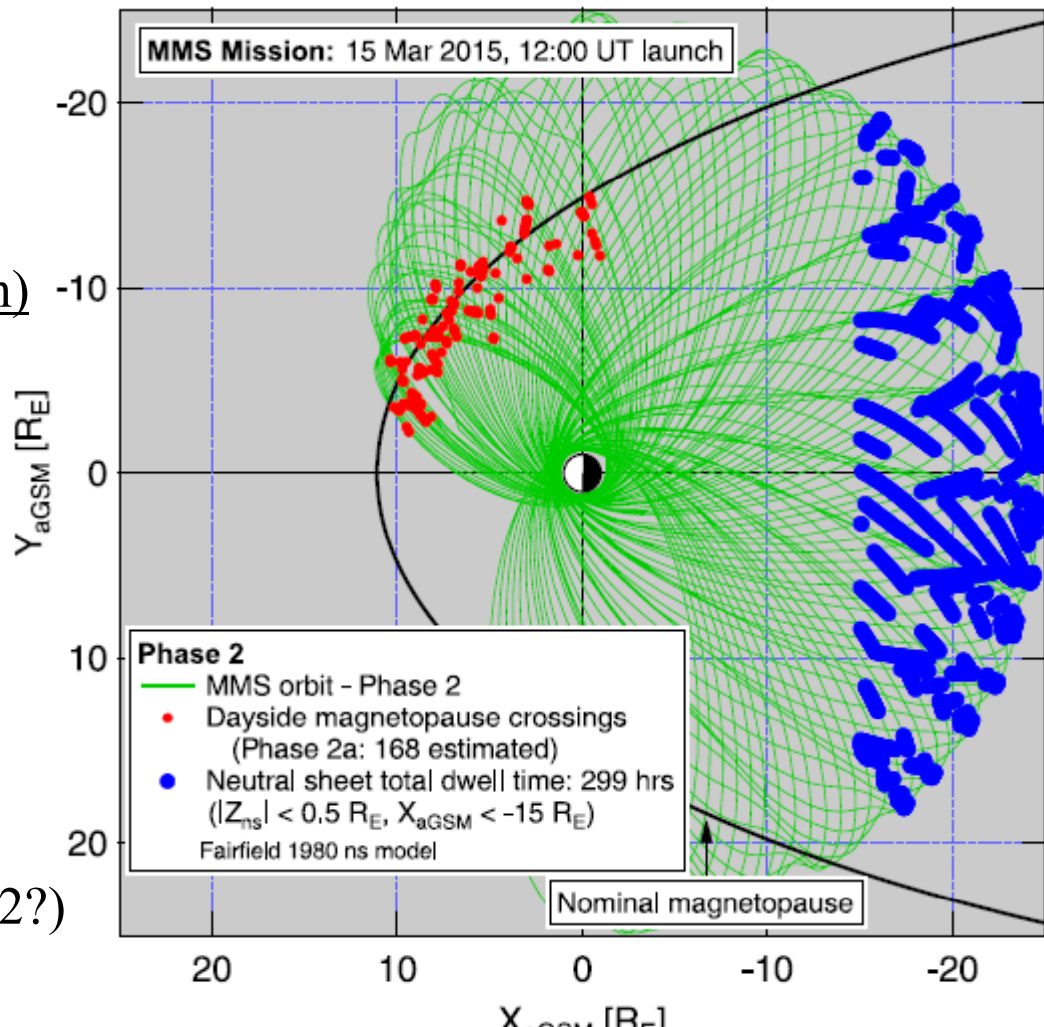
(~September, 2017–September, 2022?)

5年延長を計画中

January 5, 2019より遠地点 $\sim 28 R_E$

リコネクションやマグネットポーズ以外もターゲットになりうる

月の引力により軌道要素(傾斜角等)が徐々に変化(プラズマシート滞在時間は年々減少?)



[Fuselier et al., 2016]

◆軌道、Region Of Interest (ROI)

■Phase 2b (Magnetotail reconnection)

(May 5, 2017–August ~19, 2017?)

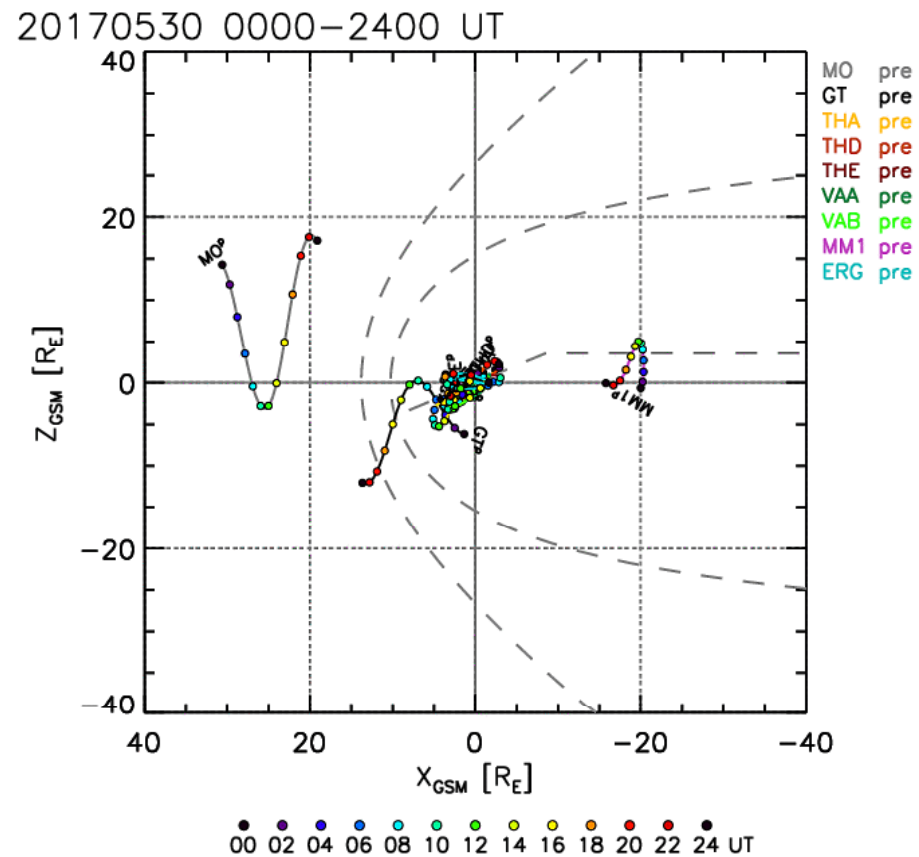
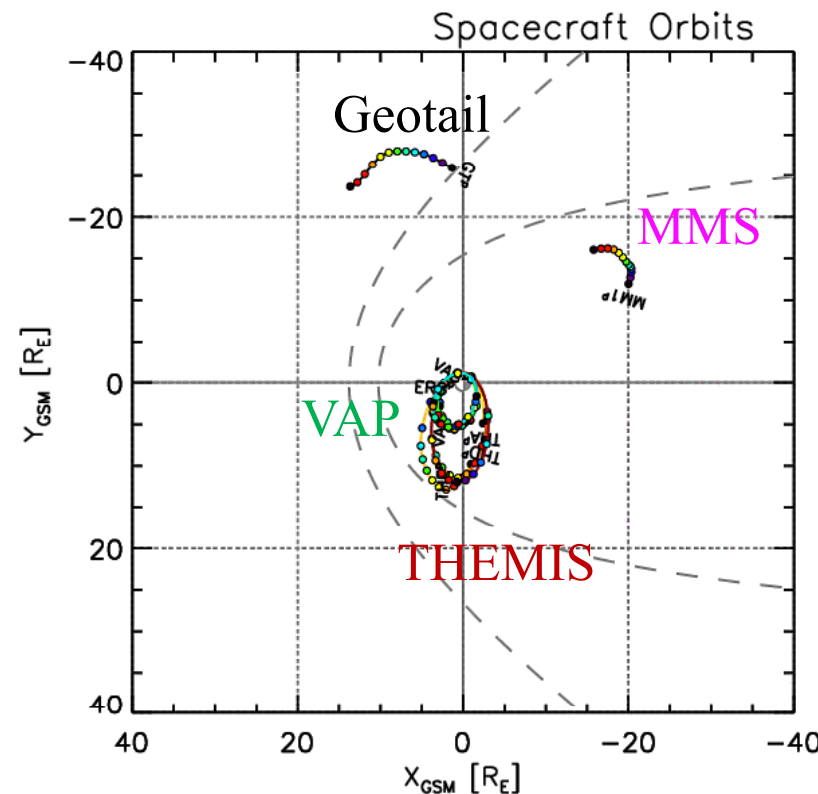
遠地点: $25 R_E$, 0300–1800 MLT

周期: ~66 h 43 min

衛星間距離

160, 40, 20, 10 kmの順でPhase-2b
開始後、約2週間ごとに縮小
(ただし実際に<30 kmが可能かはGPS
による位置決定精度に依存)

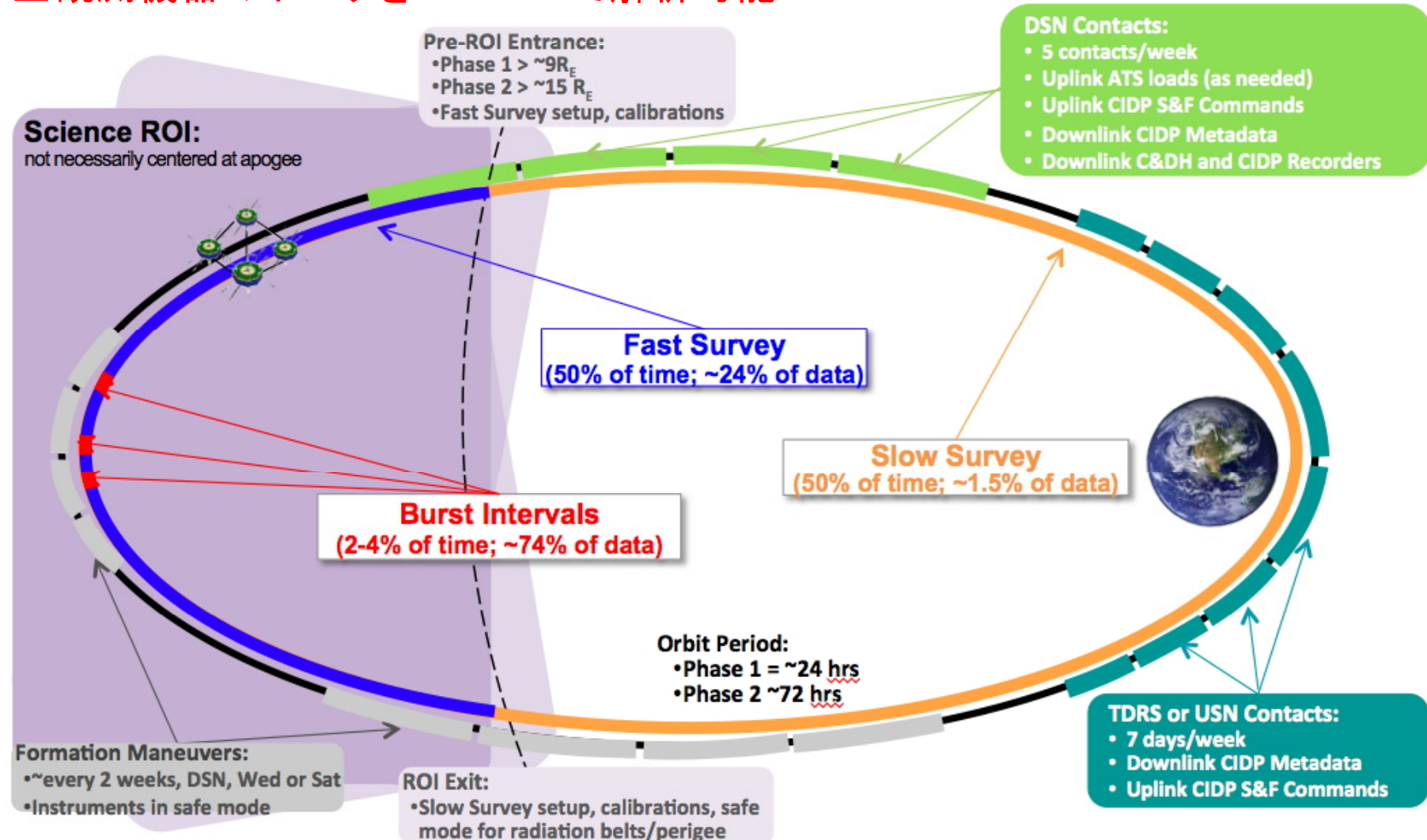
MMSの遠地点はGeotailから見てMLTで約5時間前、
THEMISから見て約9時間後ろ



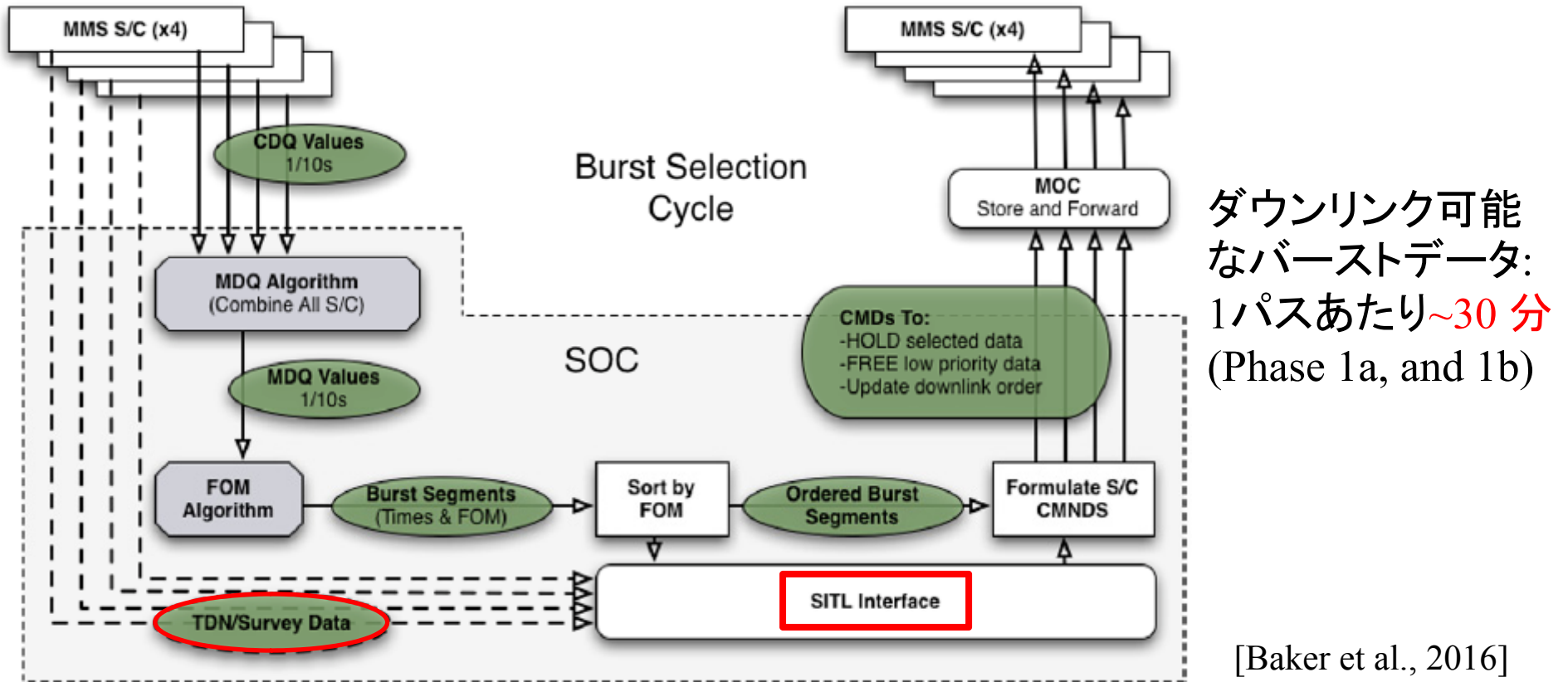
◆軌道、Region Of Interest (ROI)

16

Region Of Interest内でFast Survey(常時Burst観測)、それ以外でSlow Survey
データセンターでデータ公開中(原則、取得後30日でLevel-2を公開)
全観測機器のデータをSPEDASで解析可能



ROI(Fast Survey)では常時バースト観測をし、機上ストレージ(96 GB)に蓄積
 ダウンリンク後1時間程度でQLが作成され、Scientist In The Loop(SITL)のメンバー
 がその週の担当者を中心にデータセレクション(優先度付き、数時間以内)
 選択された時間帯は全衛星、全装置のバーストデータをダウンリンク(または保護)
 •選択されなかったバーストデータは3日程度で上書き
 •保護されたデータ保存用の領域が一杯になったら優先度の低いものから消去



2. MMS衛星群の観測機器

磁場

- Digital fluxgate magnetometer (DFG): 128 Hz sampling (Wave form)
- Analog fluxgate magnetometer (AFG): 128 Hz sampling (Wave form) ※バースト時
- Search Coil Magnetometer (SCM): 2 Hz–4 kHz (Wave form)
- Digital Signal Processor (DSP): ~10 Hz–6 kHz (Spectrum)

電場

- Spin-Plane Double Probe (SDP): DC–100 kHz (Wave form)
- Axial Double Probe (ADP): DC–100 kHz (Wave form)
- Digital Signal Processor (DSP): ~10 Hz–100 kHz (Spectrum) ※波形の周波数帯域はバースト時のもの
- Electron Drift Instrument (EDI)
- Active Spacecraft Potential Control neutralizers (ASPOC)

粒子

- (Electron Drift Instrument (EDI): 250 eV–1 keV)
- Fast Plasma Investigation (FPI)
- Dual Electron Spectrometers (FPI-DES): 10(6) eV–30 keV
- Dual Ion Spectrometers (FPI-DIS): 10(2) eV–30 keV
- Hot Plasma Composition Analyzer (HPCA): ~1 eV–40 keV (H^+ , He^{++} , He^+ , O^{++} , O^+)
- Energetic Particle Detector (EPD)
- Fly's Eye Energetic Particle Spectrometer (FEEPS):
25–550 keV (Electron), 50–600 keV (Ion)
- Energetic Ion Spectrometer (EIS)
10–680 keV (H^+), 60–960 keV (He^+ , He^{++}), 45–1200 keV (O^+), 30–1200 keV (Electron)

◆FIELDS

Digital fluxgate magnetometer (DFG)

Analog fluxgate magnetometer (AFG) [Russell et al., 2016]

DC precision and stability in ROI: 0.1 nT

※編隊観測による磁場勾配の検出のため4機全ての磁力計を精密に一致させる必要

→Level-2データではspin tone(0.05 Hz)やその高調波もほとんど除去されている

128 vectors/s (Burst)

16 vectors/s (Fast), 8 vectors/s (Slow)

Resolution: 24 bits

Range:

± 650 nT(Low), $\pm 10,500$ nT(High) (DFG)

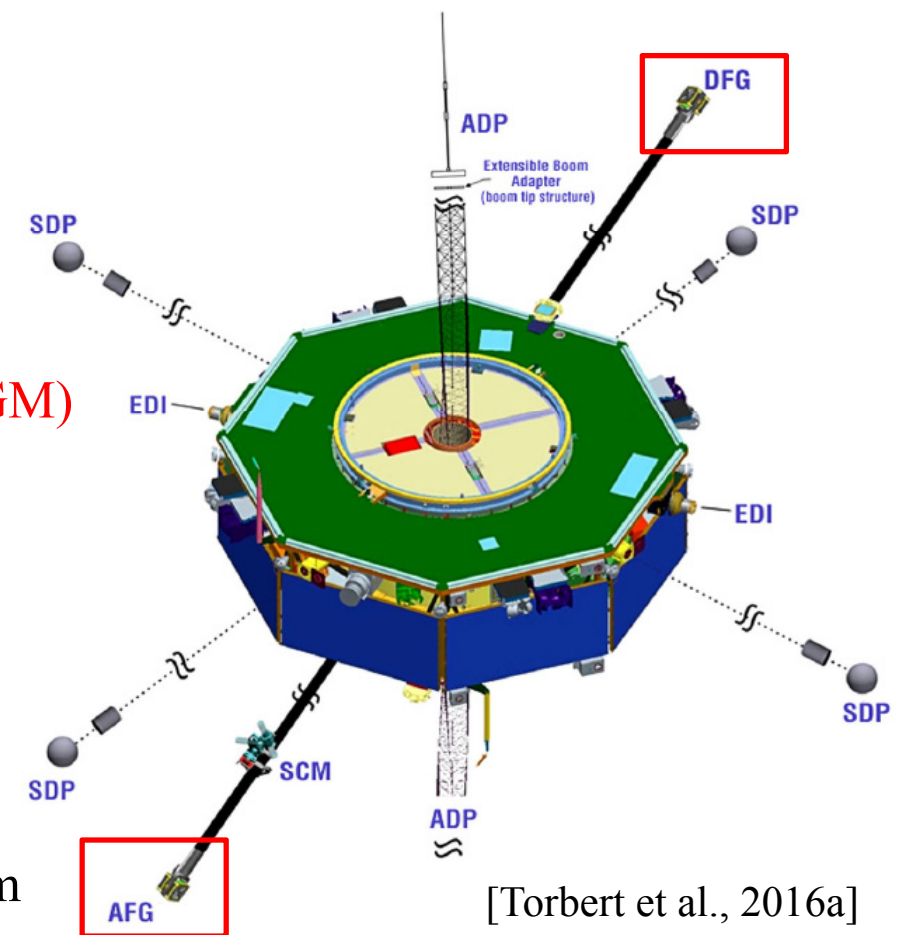
± 510 nT(Low), ± 8200 nT(High) (AFG)

Level-2ではデータを組み合わせて提供(FGM)



[Russell et al., 2015]

Boom: 5 m



[Torbert et al., 2016a]

DFGはUCLA, AFGはAustrian Academy of Scienceが中心に担当

◆FIELDS

20

Search Coil Magnetometer (SCM) [Le Contel et al., 2016]

Frequency range: **2 Hz–6 kHz**

AC: 4×10^{-10} – 10^2 nT²/Hz at 1 kHz

16,384 vectors/s (for Digital Signal Processor)

Wave form (vectors/s):

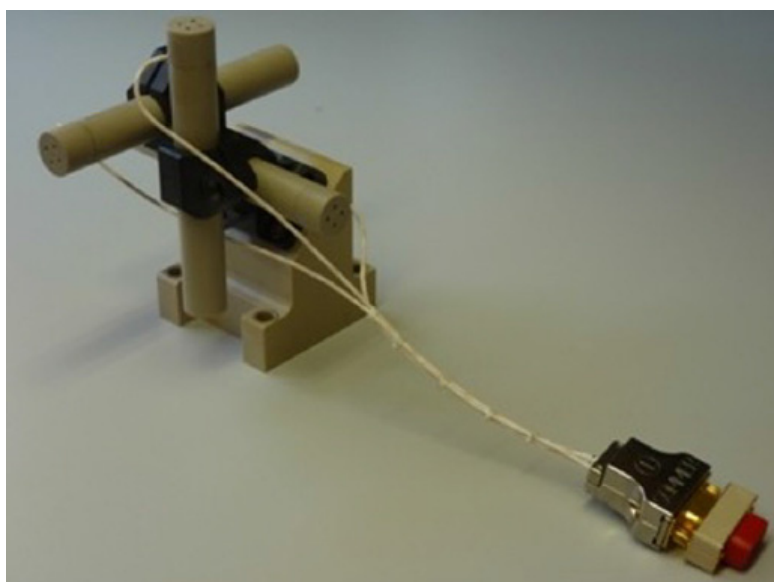
8 (Slow), 32 (Fast), 8192 (Burst), 16,384 (High-Burst)

Sensitivity:

2 pT/(Hz)^{1/2} at 10 Hz

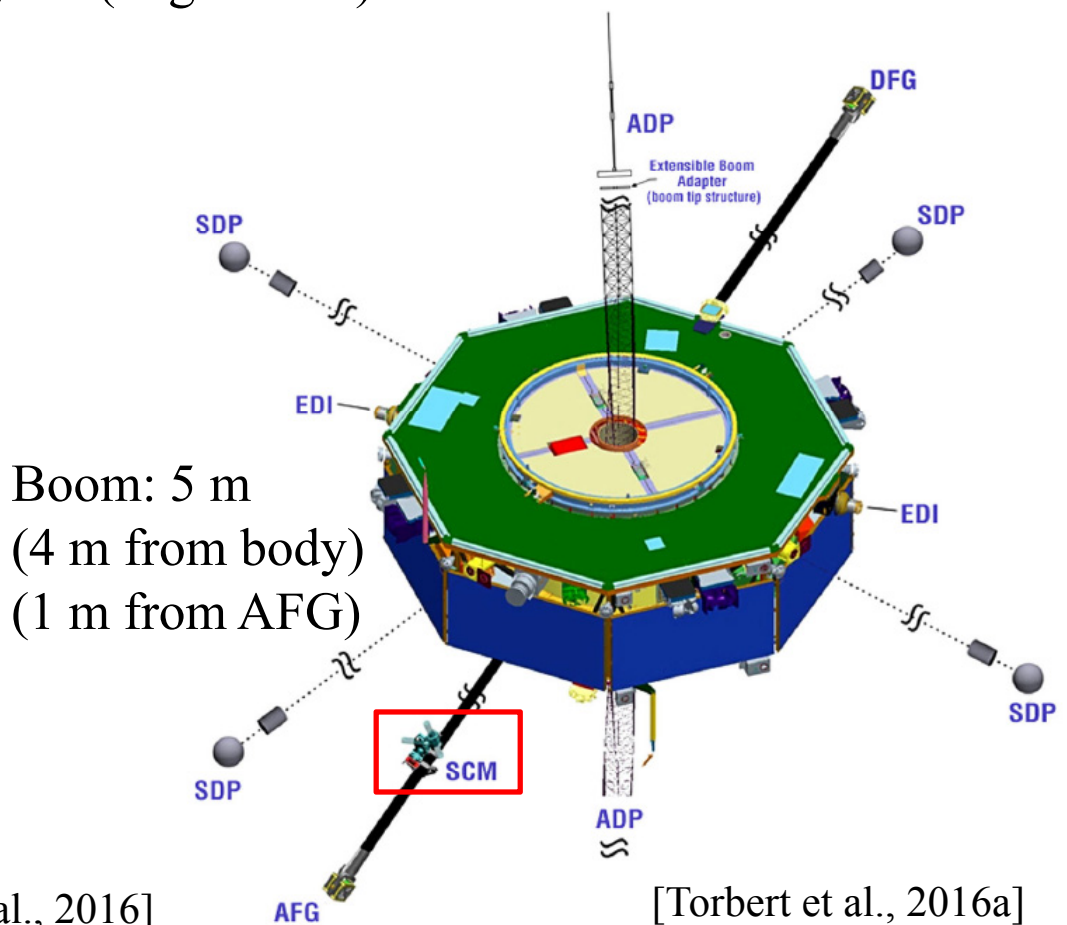
0.18 pT/(Hz)^{1/2} at 100 Hz

0.025 pT/(Hz)^{1/2} at 1 kHz



[Le Contel et al., 2016]

主要メンバー(フランスのCNRS)はTHEMISとほぼ同じやや軽量なわりにわずかに性能も劣る



[Torbert et al., 2016a]

◆FIELDS

Digital Signal Processor (DSP) [Torbert et al., 2016a; Ergun et al., 2016]

B-field from SCM (16,384 vectors/s)

Frequency range: **2 Hz–6 kHz**

AC: 4×10^{-10} – 10^2 nT²/Hz at 1 kHz

1024-point FFT

56 frequency steps

8–120 Hz (8 steps, $\Delta f = 16$ Hz)

136–7936 Hz (48 steps, $\Delta f/f = 6.5\%–12\%$)

Slow: 16 sec-averaged spectrum (2 components?)

Fast: 2 sec-averaged spectrum?

Burstは波形データがあるため、DSPデータ(スペクトル)は無い

電場(次ページ以降)についてもDSPを使用

◆FIELDS

Spin-Plane Double Probe (SDP) [Lindqvist et al., 2016]

Probe-probe distance: 120.92 m

Frequency range: DC–100 kHz

DC precision: 0.5 mV/m

Resolution: 0.05 mV/m

Range: ± 625 mV/m

AC: 9×10^{-16} – 10^{-4} (V/m)²/Hz at 10 kHz

Axial Double Probe (ADP) [Ergun et al., 2016]

Tip-to-tip distance: 30.4 m

Frequency range: DC–100 kHz

DC precision: ~1 mV/m

Resolution: 0.026 mV/m

Range: ± 800 mV/m

AC: 4×10^{-14} – 10^{-3} (V/m)²/Hz at 10 kHz

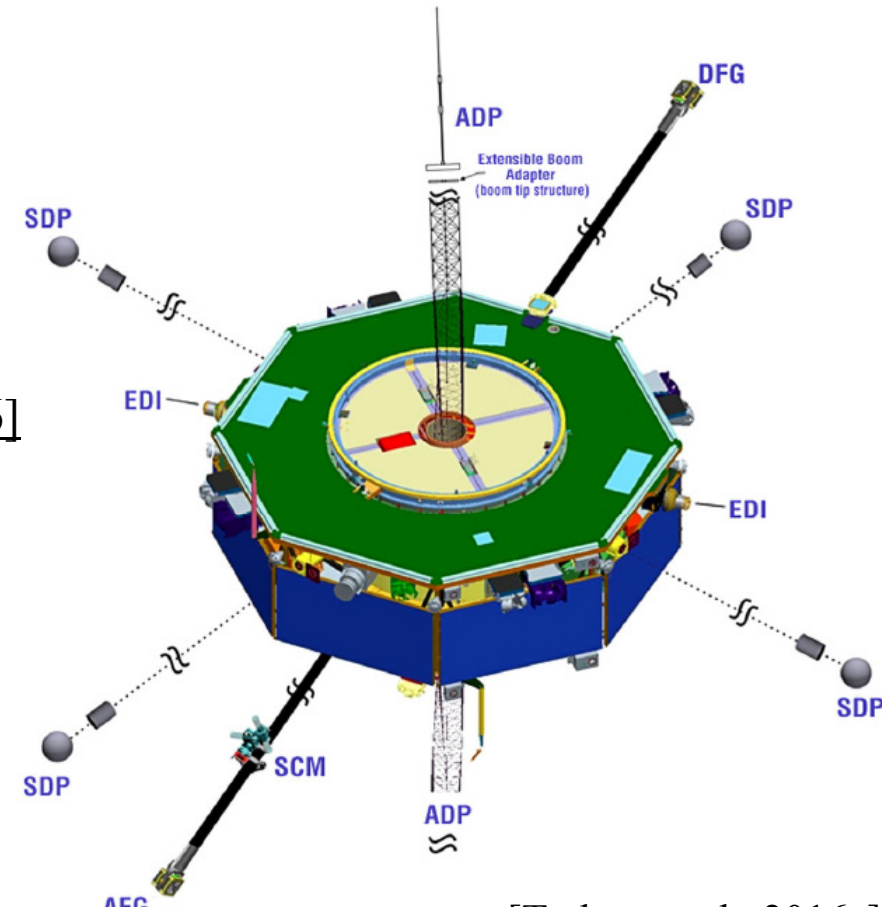
SDP, ADP (Wave form, Samples/s)

16,384 (DC-Efield, Probe voltage for Digital Signal Processor)

262,144 (AC-Efield for Digital Signal Processor, 6.25% duty cycle)

8 (Slow), 32 (Fast), 8192 (Burst), 65,536(High-Burst)

(High-Burstは8秒あたり2秒の断続的な観測)



[Torbert et al., 2016a]

◆FIELDS

Spin-Plane Double Probe (SDP) [Lindqvist et al., 2016]

Probe-probe distance: 120.92 m

Frequency range: DC–100 kHz

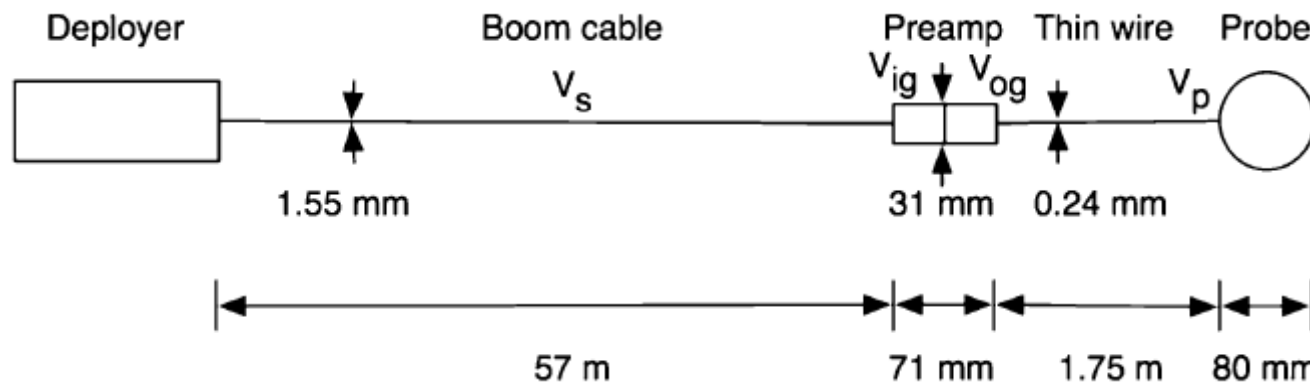
DC precision: 0.5 mV/m

Resolution: 0.05 mV/m

Range: ± 625 mV/m

AC: 9×10^{-16} – 10^{-4} (V/m) 2 /Hz
at 10 kHz

Viking, Freja, Astrid-2, Clusterと類似
(ただし、Langmuir modeは非採用)



[Lindqvist et al., 2016]

80 mm球プローブ
(Titanium nitride)

- 時刻により、ウェイク、衛星電位コントロールの影響が大きい場合あり
- June 12, 2016よりMMS4のプローブのうち1つのバイアス電流供給部分が故障し、以降はMMS4のDC電場データは3プローブのみから導出中

◆FIELDS

24

Axial Double Probe (ADP) [Ergun et al., 2016]

Tip-to-tip distance: 30.4 m

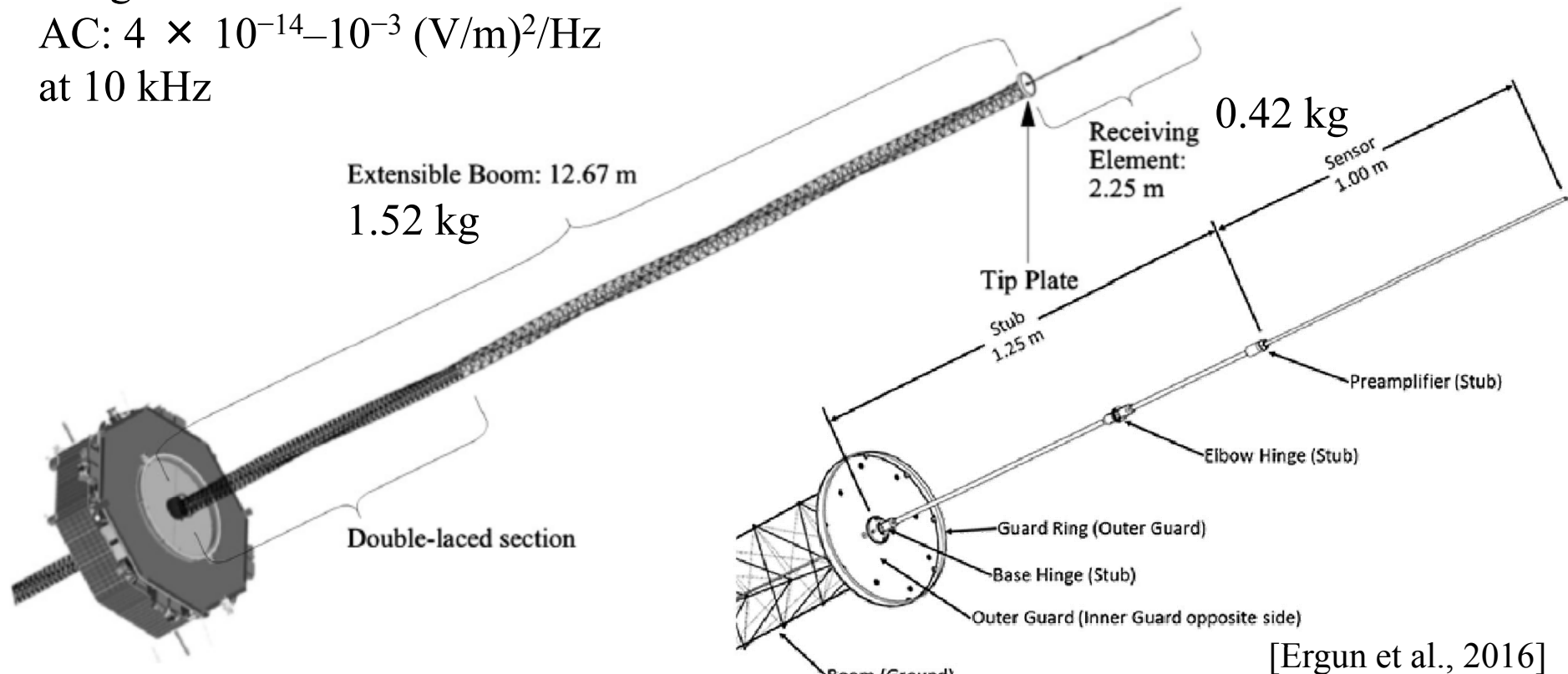
Frequency range: DC–100 kHz

DC precision: ~1 mV/m

Resolution: 0.026 mV/m

Range: ±800 mV/m

AC: 4×10^{-14} – 10^{-3} (V/m) 2 /Hz
at 10 kHz



[Ergun et al., 2016]

最長の軸方向プローブ(Electron diffusion regionにおける $E_{||}$ の測定のため)
(THEMIS: ~6.9 m [Bonnell et al., 2008], Van Allen Probes: ~15 m [Wygant et al., 2013])

Digital Signal Processor (DSP) [Torbert et al., 2016a; Ergun et al., 2016]**Table 5** Summary of spectral processing and sensitivities

| Signal | Analog filtering | | Digital processing | | | | | Power spectral density ¹ | |
|-----------------|------------------|-----------|--------------------------|-----------------|--------------------|--------------|-----------------------------|-------------------------------------|---------------------------------|
| | Low (Hz) | High (Hz) | Sample rate (s^{-1}) | Freq. min. (Hz) | Freq. max. (Hz) | # Freq. bins | ($\delta f/f$) | Receiver sensitivity ($V/m)^2/Hz$ | Narrow band range ($V/m)^2/Hz$ |
| E12; E34 | DC | 6500 | 16384 | 8 | 120 | 8 | $\delta f = 16 \text{ Hz}$ | 8×10^{-13} | 5×10^{-3} |
| | | | | 136 | 7936 | 48 | 6.5 %–12 % | | |
| E56 | (as above) | | (as above) | | | | | 2×10^{-12} | 6×10^{-2} |
| V1 to V4 | (as above) | | (as above) | | | | | 1.5×10^{-11} | 5×10^{-3} |
| V5; V6 | (as above) | | (as above) | | | | | 1.5×10^{-10} | 6×10^{-2} |
| E12ac; E34ac | 100 | 10^5 | 2.62×10^5 | 128 | 1920 | 8 | $\delta f = 256 \text{ Hz}$ | 6×10^{-16} | 10^{-4} |
| | | | | 2176 | 1.26×10^5 | 48 | 6.5 %–12 % | | |
| E56ac | (as above) | | (as above) | | | | | 8×10^{-15} | 10^{-3} |
| V1ac; V2ac | (as above) | | (as above) | | | | | 6×10^{-16} | 10^{-4} |

1, 2, 3, 4

SDP

5, 6

ADP

AC: >100 Hz
(high pass
filtered
signal)

1024-point FFT (56 frequency steps)

[Ergun et al., 2016]

Slow: 16 sec-averaged spectrum (2 components)

Fast: 2 sec-averaged spectrum

High Speed Burst
Solitary Structure Detector

◆FIELDS

26

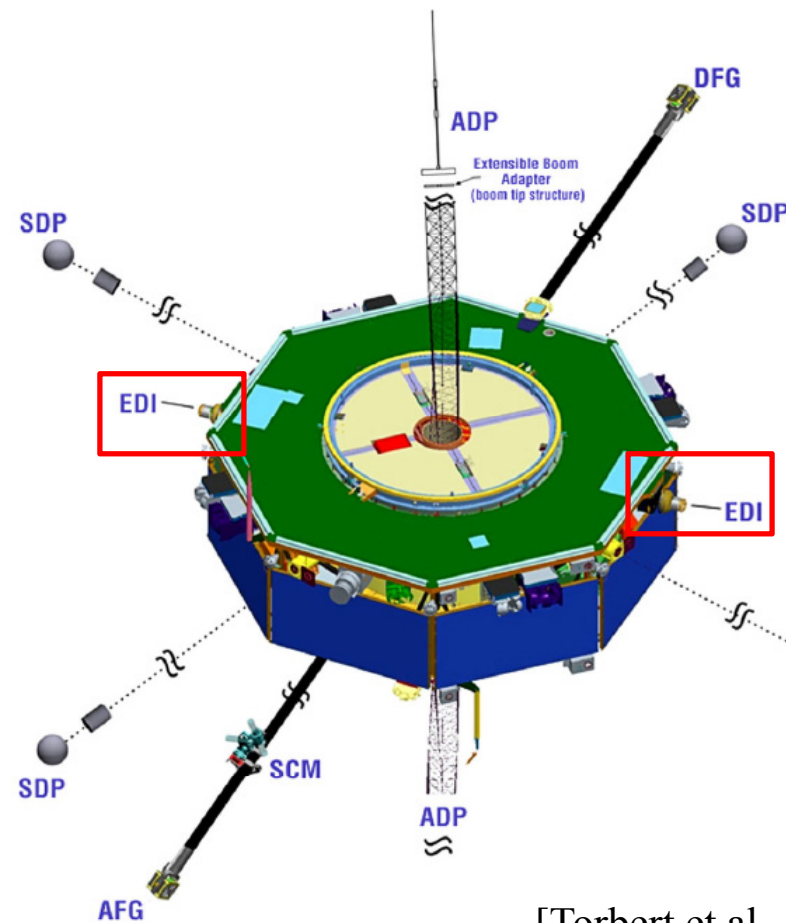
Electron Drift Instrument (EDI) [Torbert et al., 2016b]

半球をカバーする粒子計測機と電子ビーム発射機構

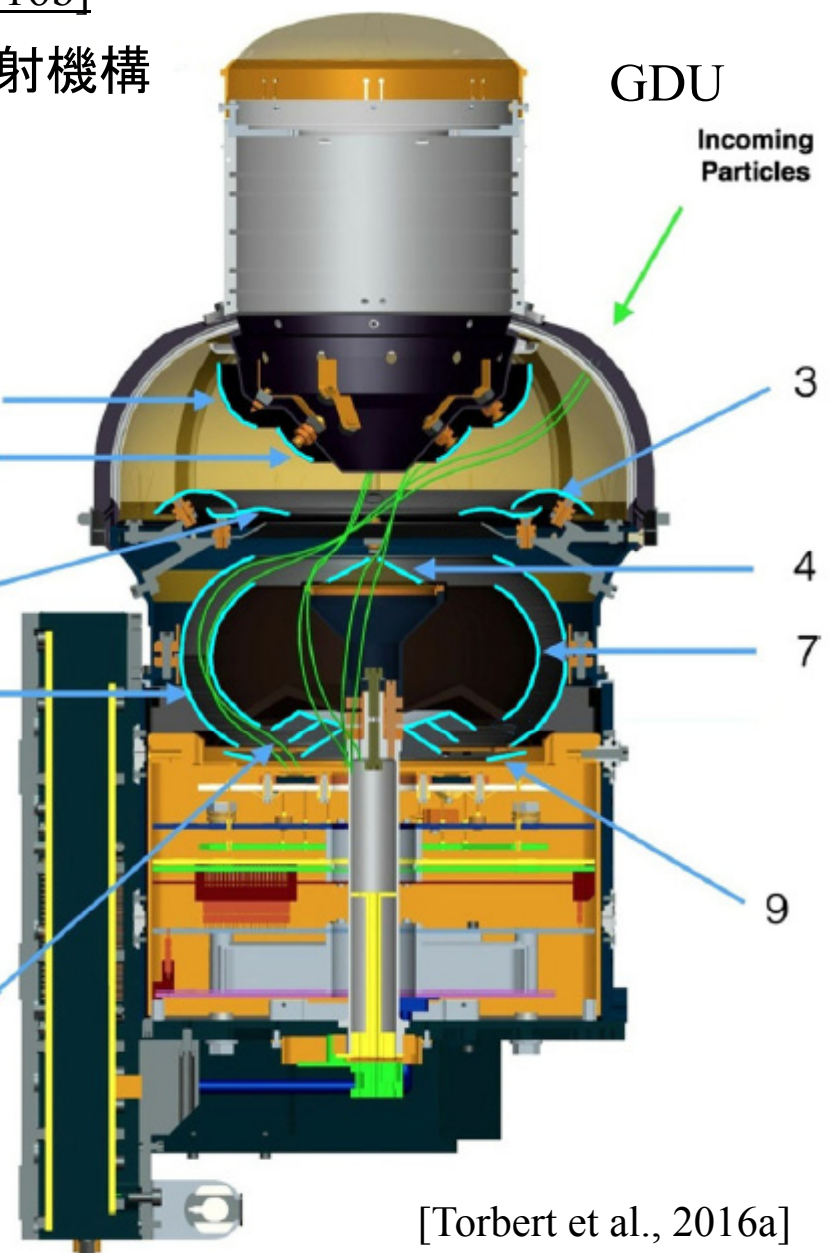
(Gun Detector Unit (GDU))

2台で全天をカバー

検出部は360°を32セクターに分割(11.25°ごと)



Electron Gun



Electron Drift Instrument (EDI) [Torbert et al., 2016b]

Electric field mode (Windshield-Wiper mode):

磁力線垂直方向(128 Hz磁場データから検出)に2本の変調をかけた(65 kHz–4 MHz)電子ビーム(0.25–1.0 keV)を打ち、受信できる角度、時間差から磁力線垂直方向の電場を推定

Slow, Fast: ~16 Hz

Burst: ~125 Hz

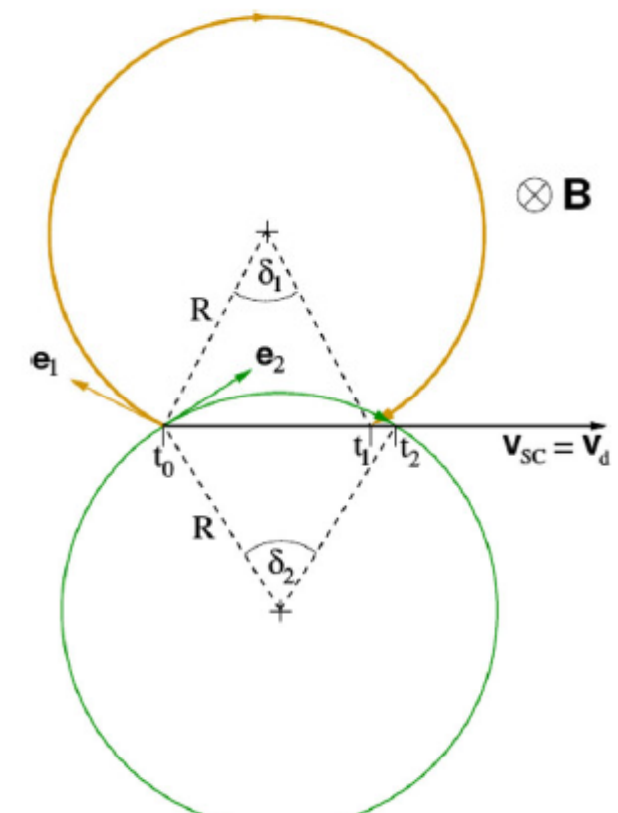
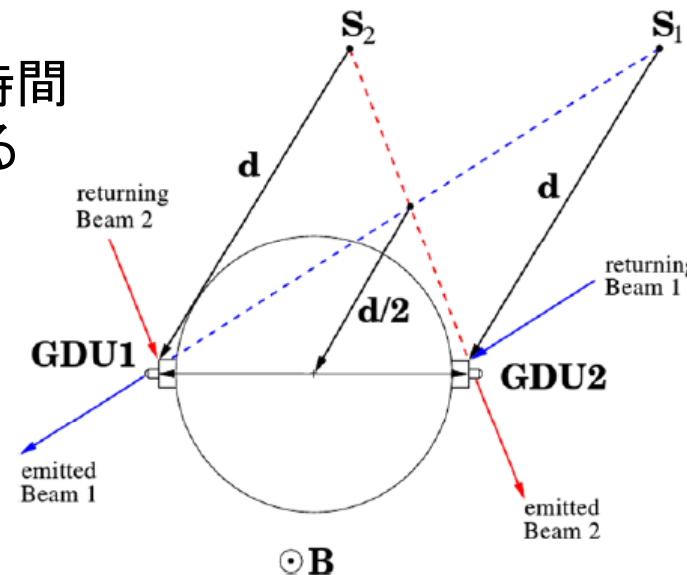
電場強度の精度: 0.1 mV/m

磁場強度: $\pm 0.1\%$ (at 30 nT, AFG, DFG較正に使用)

※磁場が弱くなりすぎたり、電場変動が激しすぎると
ビームが戻って来なくなるため使用できない

電場推定はより低い時間分解能で行われている
(~5 sec?)

Electric field mode
での観測時間は
ROIの一部のみ



[Torbert et al., 2016b]

Electron Drift Instrument (EDI) [Torbert et al., 2016b]

Ambient mode:

磁場方向を追跡(128 Hz磁場データから検出)し、
平行、反平行方向の電子を超高時間分解能で
計測

(エネルギー固定: 250, 500, 1000 eVから選択)
※他の任意の方向も設定可能

Slow:

31.25 ms (32 Hz)

※断続的に数分に1度、数秒間のみ

Fast:

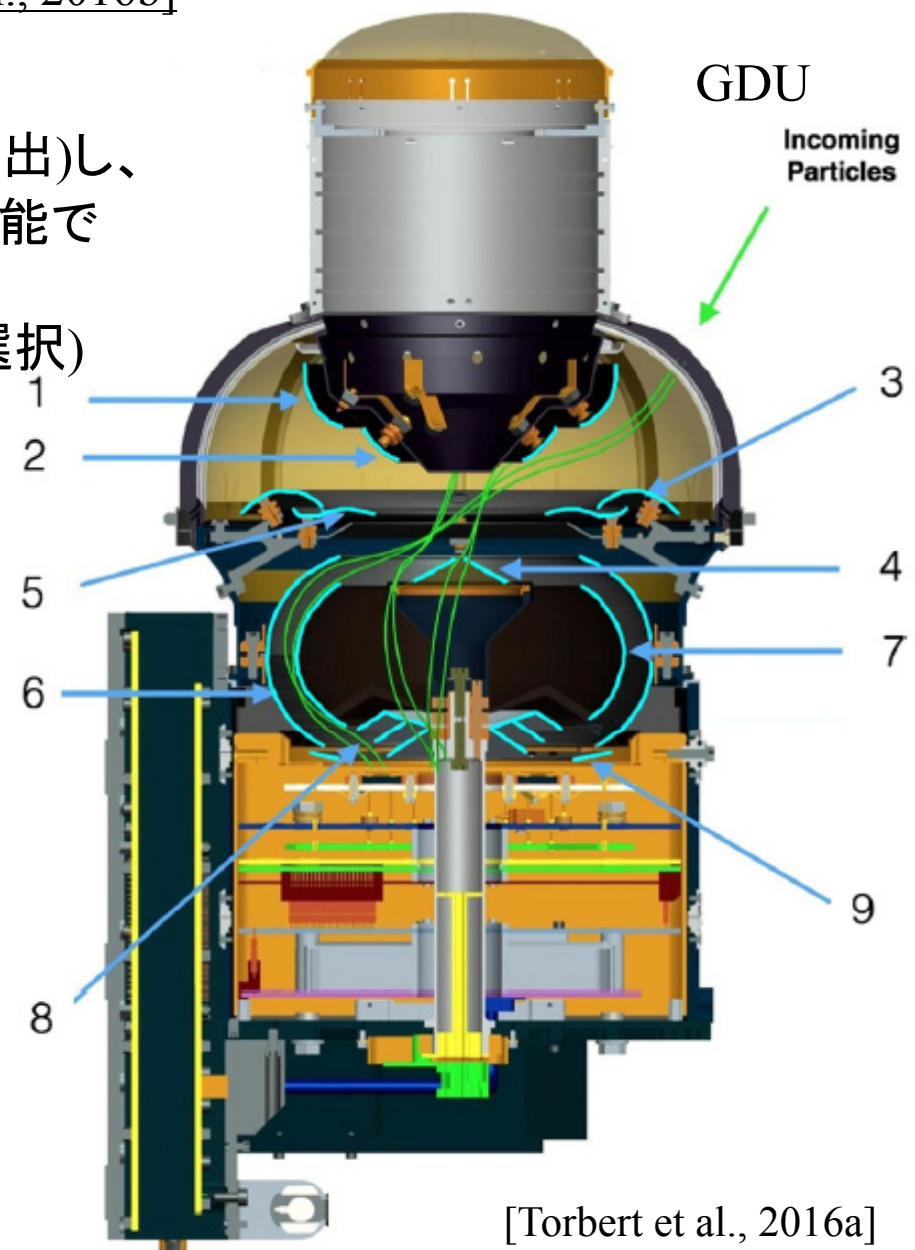
31.25 ms (32 Hz) (ROI内連続観測)

Burst:

~1 ms (1024 Hz)

(Burstのみ磁力線平行、反平行だけ
でなく、それぞれ付近の3セクターの
データ(合計8方向)を伝送)

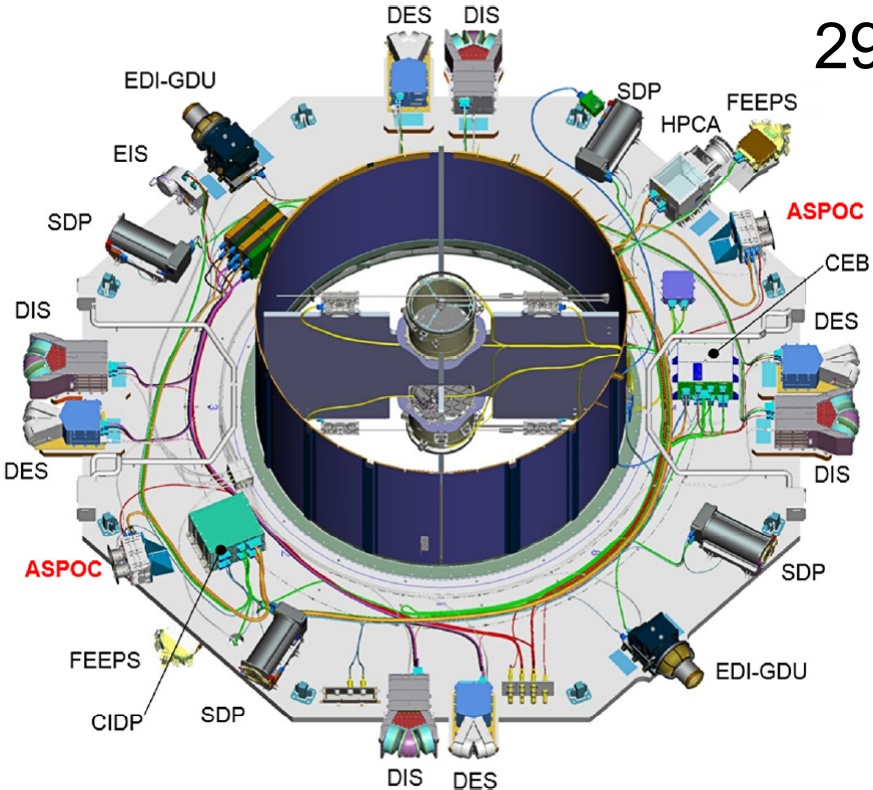
ROIの半分以上ではこの
Ambient modeで観測



[Torbert et al., 2016a]

Active Spacecraft Potential Control
neutralizers (ASPOC) [Torkar et al., 2016]

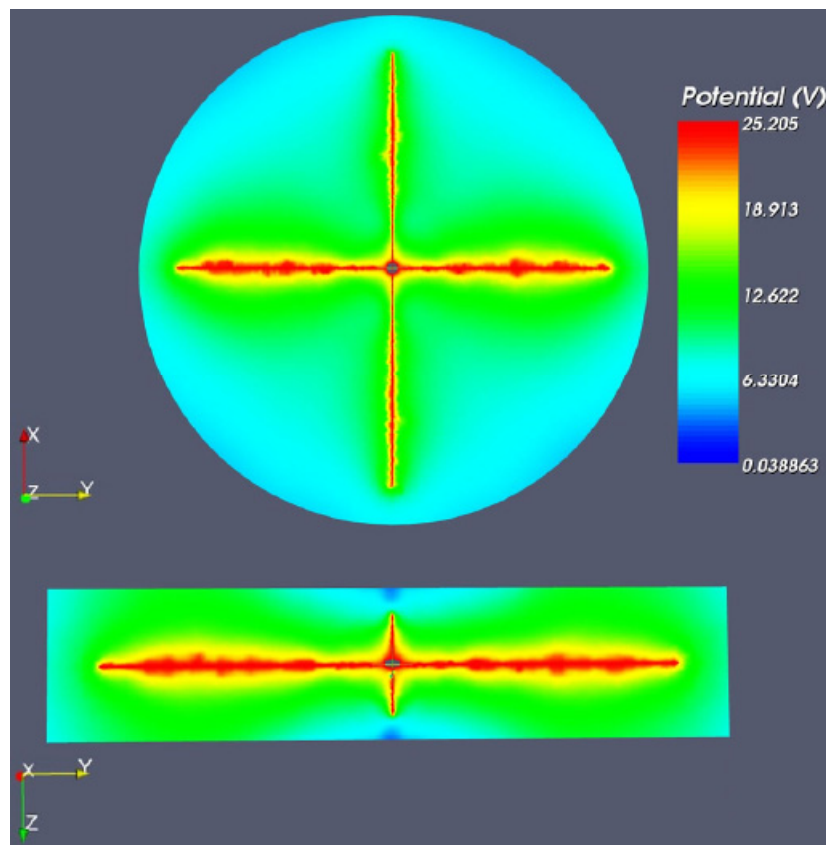
各衛星2基搭載(イオン源各4)
Indium+を5–8 keV (max. 12 keV)
に加速して発射
 $10 \mu\text{A} \times 2 (\sim 25,000 \text{ h} \times 4)$
衛星電位: ~2 V (Probes–衛星)



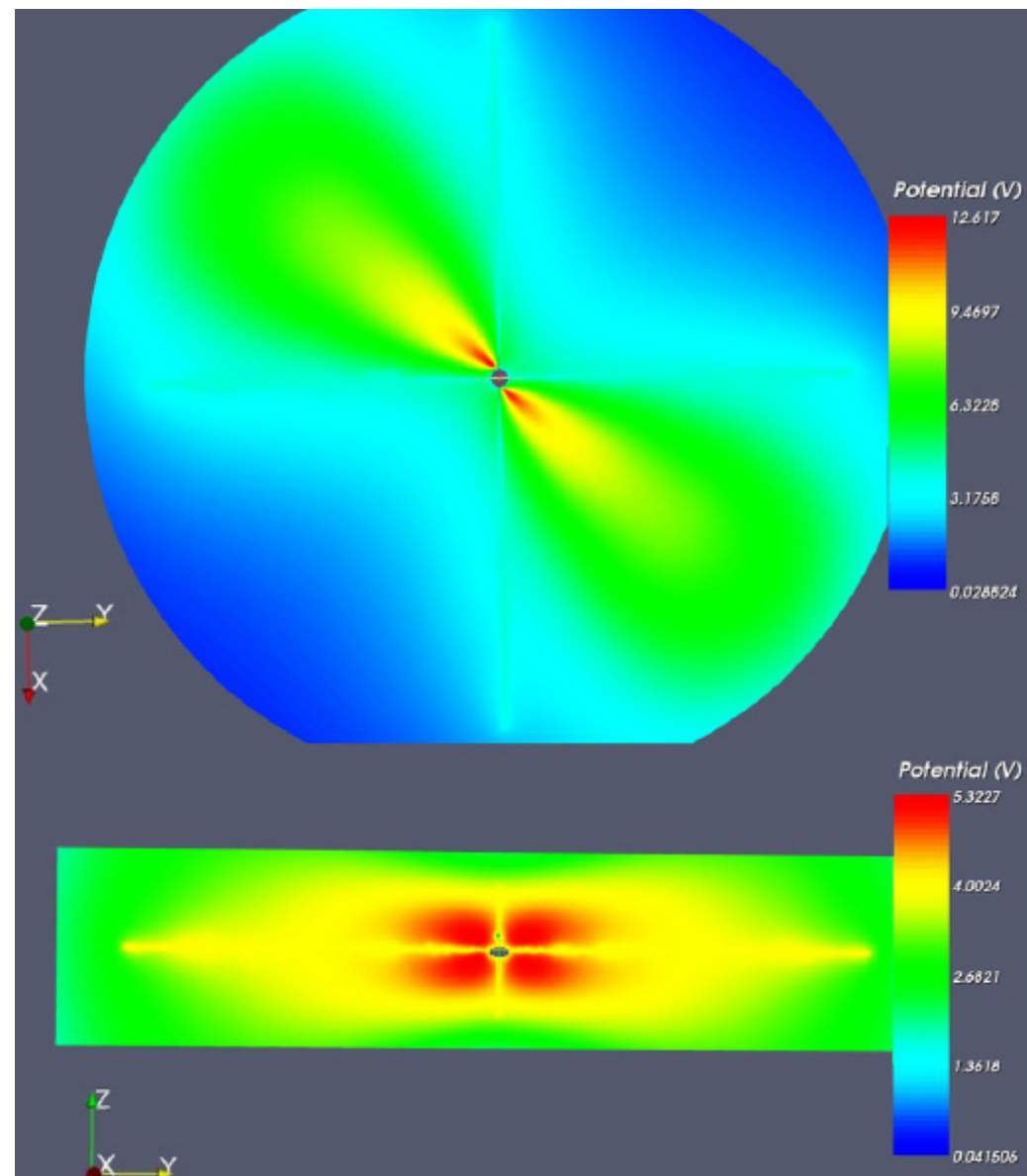
| Acronym | Full name | Remarks | [Torkar et al., 2016] |
|---------|--|--|-----------------------|
| ASPOC | Active Spacecraft Potential Control | | |
| CEB | Central Electronics Box | For the FIELDS instrument suite | |
| CIDP | Central Instrument Data Processor | For the scientific payload | |
| DES | Dual Electron Spectrometer | Part of the Fast Plasma Instrument | |
| DIS | Dual Ion Spectrometer | Part of the Fast Plasma Instrument | |
| EDI-GDU | Electron Drift Instrument, Gun-Detector Unit | | |
| EIS | Energetic Ion Spectrometer | Part of the Energetic Particle Detectors | |
| FEEPS | Fly's Eye Energetic Particle Sensors | Part of the Energetic Particle Detectors | |
| HPCA | Hot Plasma Composition Analyzer | | |
| SDP | Spin-Plane Double Probe | Part of FIELDS, for electric field and spacecraft potential measurements | |

Active Spacecraft Potential Control neutralizers (ASPOC) [Torkar et al., 2016]

2本のイオンビームによって
数10 Vの帶電を数Vに軽減
→低エネルギープラズマと電
場の正確な計測を可能に



[Torkar et al., 2016]

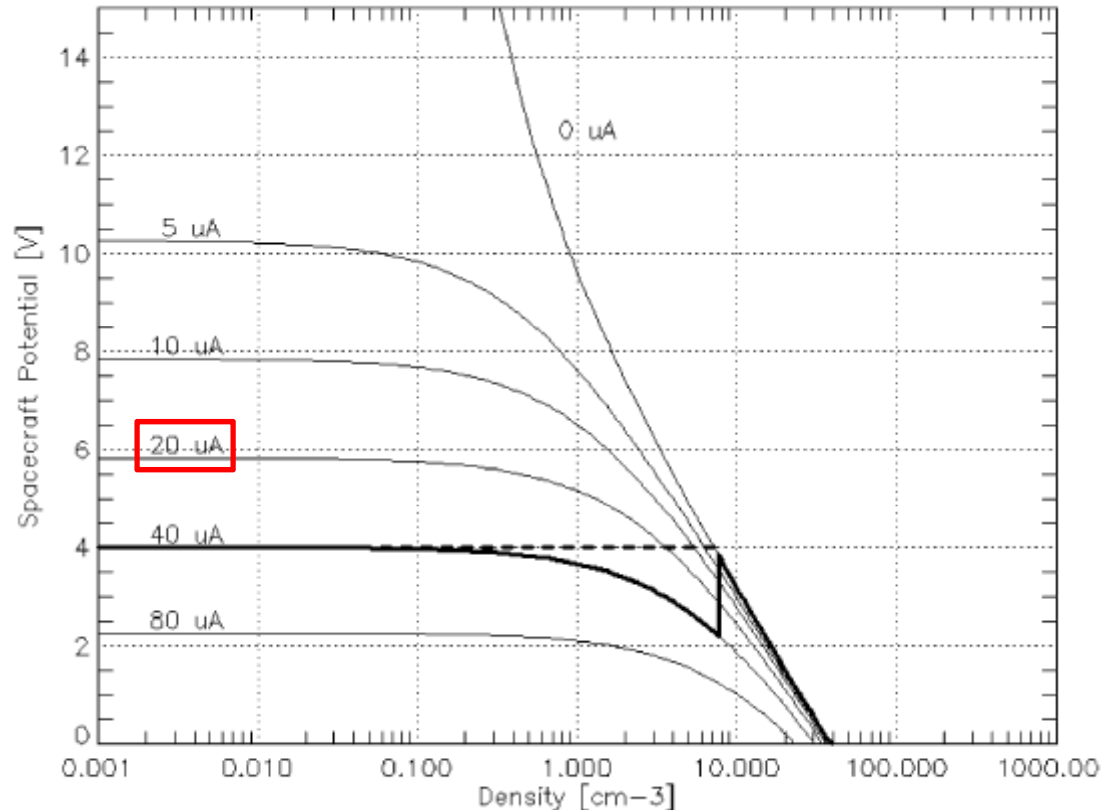


Active Spacecraft Potential Control neutralizers (ASPOC) [Torkar et al., 2016]

当初の計画では $20 \mu\text{A} \times 2$ で運用予定だったが、試験観測でDC付近の電場観測に影響が出てしまう事が明らかになつたため、Phase-1a開始以降は $10 \mu\text{A} \times 2$ で運用

Phase-1a初期はROI内で全機同時運用であったが、October 12, 2015以降はROIの一部のみで全機同時、またはROI内を4分割して1衛星ずつのローテーションで運用

ACPOC稼働時の衛星電位は打ち上げ前の想定(右図)よりやや低い(**低密度でも約4 V**)



Estimated effect of ion beams on the spacecraft potential of MMS [Torkar et al., 2016]

シース等の高密度の領域では運用しても効果は薄い

◆Particle

Fast Plasma Investigation (FPI)
Dual Electron Spectrometers (FPI-DES)
Dual Ion Spectrometers (FPI-DIS)

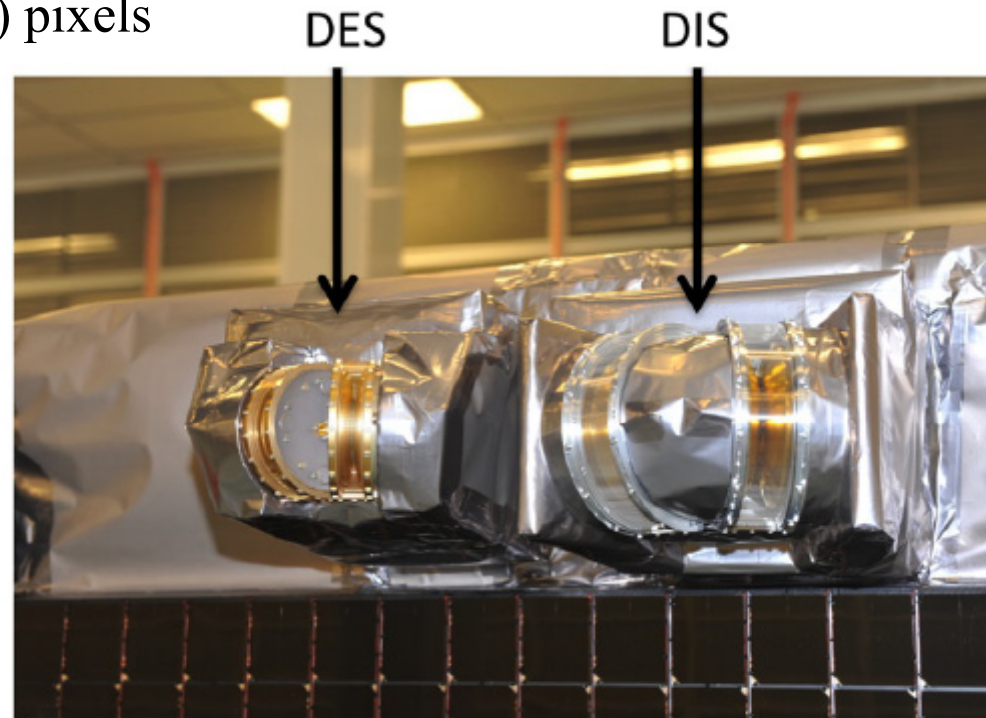
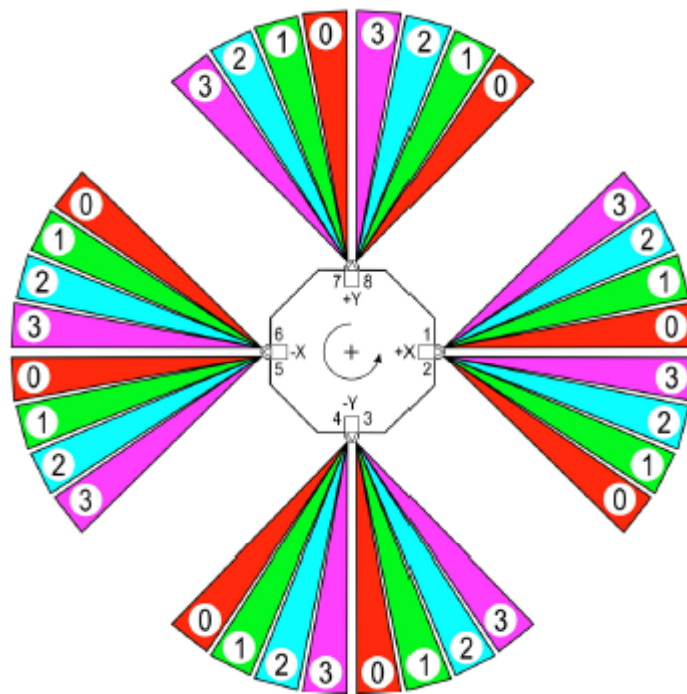
DESはNASA/GSFC、DISは
ISAS/JAXAが中心に担当

スピニに頼らずに超高時間分解能で3次元分布関数を取得する
各衛星4基ずつのDESとDIS(各8 heads)

Energy range: ~10 eV–30 keV (32 (64) energy bins)

※Phase-1bからは10 eV以下のキャリブレーションは不十分ながら、イオンは2 eV、
電子は6 eVより計測(Level-2のモーメント計算には>10 eVのみ使用予定)

32 (Azimuth) × 16 (Elevation) (=512) pixels



[Pollock et al., 2016]

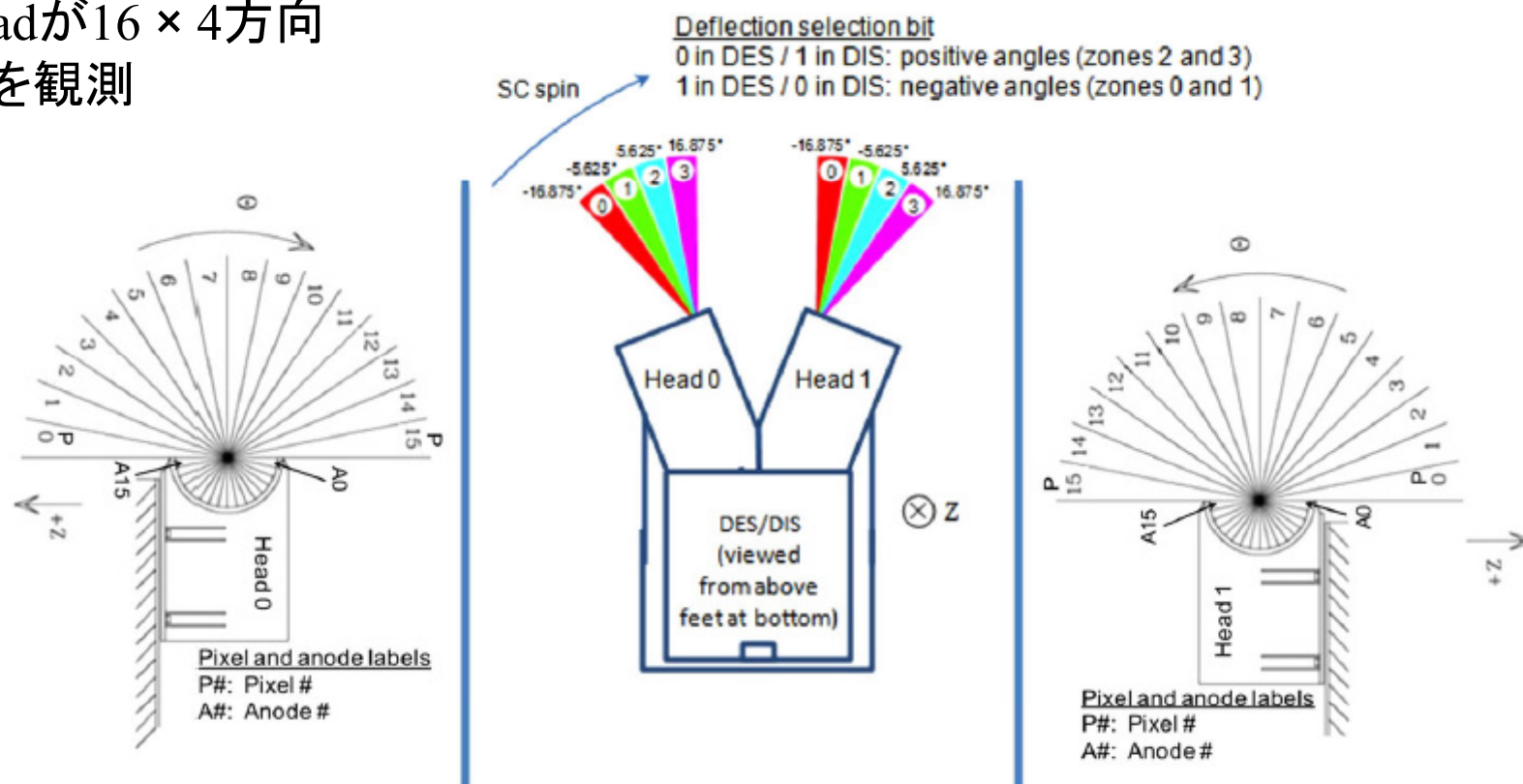
Fast Plasma Investigation (FPI)
Dual Electron Spectrometers (FPI-DES)
Dual Ion Spectrometers (FPI-DIS)

32 (Azimuth) \times 16 (Elevation) (=512) pixels
 11.25° (Azimuth) \times 11.25° (Elevation)

各headが 16×4 方向
ずつを観測

DESはNASA/GSFC、DISは
ISAS/JAXAが中心に担当

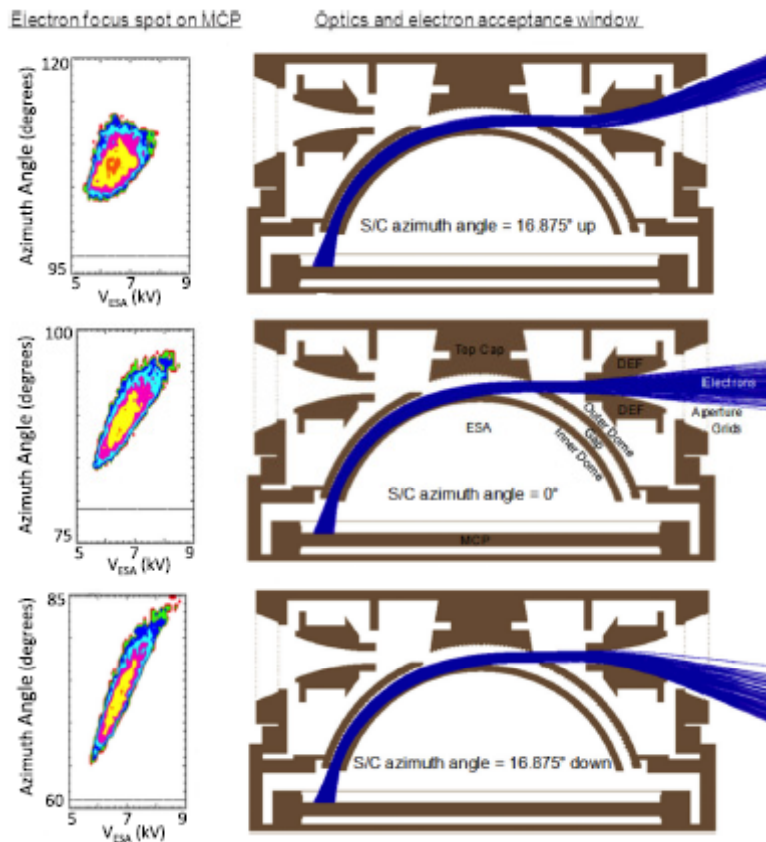
THEMISは88 pixels (磁気圏
では 22.5° 程度の角度分解能)



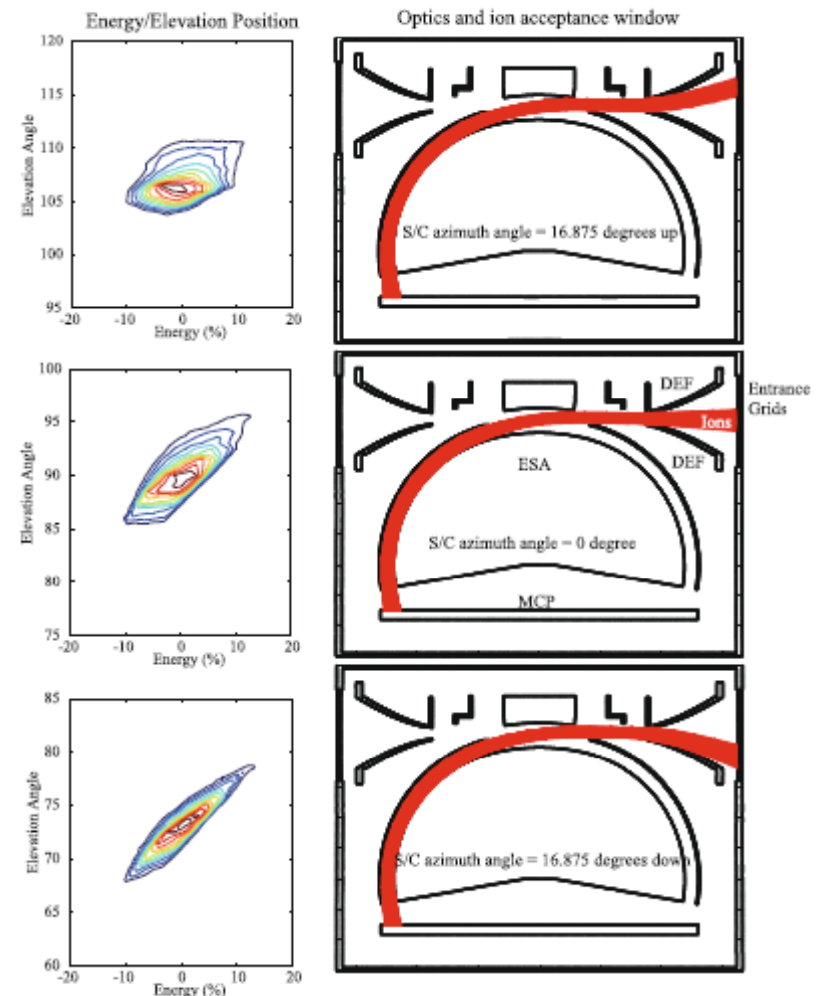
[Pollock et al., 2016]

Fast Plasma Investigation (FPI)
Dual Electron Spectrometers (FPI-DES)
Dual Ion Spectrometers (FPI-DIS)

DES



DIS



Examples of DES and DIS ray-trace simulation results of the energy and angle response

[Pollock et al., 2016]

◆Particle

Fast Plasma Investigation (FPI)
Dual Electron Spectrometers (FPI-DES)
Dual Ion Spectrometers (FPI-DIS)

時間分解能:

DES: 0.03 (0.06) sec (33.3 (16.7) Hz)
 DIS: 0.15 (0.30) sec (6.67 (3.33) Hz)

THEMISのESAの時間分解能は3秒

(電子(イオン)は100(20)倍)

GeotailのLEPの時間分解能は12秒

Phase-1aまでは右図のように64エネルギーステップのうち偶数番目と奇数番目を交互に計測
 (括弧内は64エネルギーステップの場合の時間分解能)

Phase-1bからはモーメントの振動を抑えるため、32エネルギーステップで固定して計測に変更

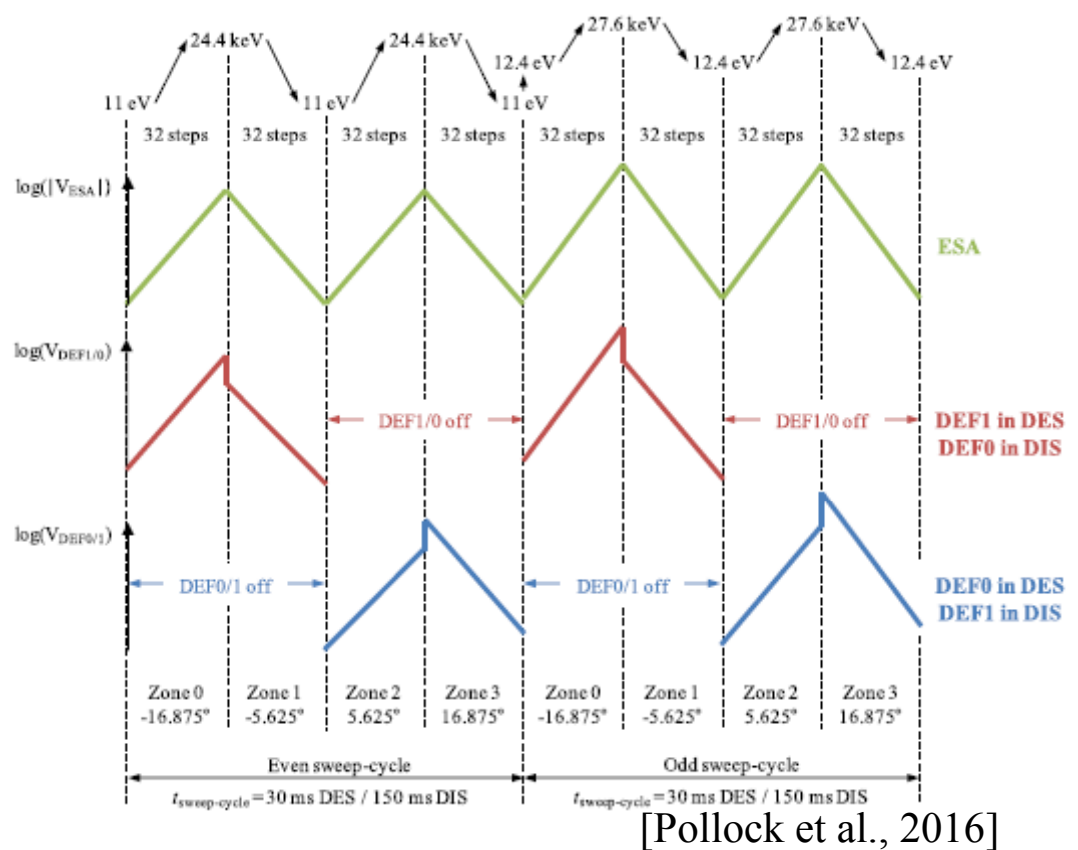
一部データ(特にシースでの電子が多い)に不可逆圧縮がかかっているため詳細な解析時は圧縮について確認が必要(尾部ではほぼ不可逆圧縮なし?)

$$32 \text{ (Energy)} \times 32 \text{ (Azimuth)} \times 16 \text{ (Elevation)} = 16,384$$

磁場強度40 nTの場合のプロトンサイクロトロン周波数:

0.6 Hz (<< DISの時間分解能)

1エネルギーSTEPあたりの積分時間:
 0.195 ms (DES)、1.00 ms (DIS)



Fast Plasma Investigation (FPI)

Dual Electron Spectrometers (FPI-DES)

Dual Ion Spectrometers (FPI-DIS)

時間分解能:

Fast: 4.5 sec (バーストデータを内部で平均)

Slow: 60 sec (DES, DISそれぞれ1台ずつのみ使用して、全天をスキャンして
3 spin平均、方位角方向は32から16 sectorへ半減(データ未公開))

分布関数に不可逆圧縮をかけて通信量を節約しているため、ノイズのような
ものが発生し、詳細な解析には向かない

THEMISのESAの時間分解能は3秒

※THEMISは3秒で全天をスキャンするのに対して、MMSのSurvey dataは全天データを
常時取りながら平均

→MMSのSurvey dataではこれ以上の分解能にデータをばらすことはできない

Fast:

$$32 \text{ (Energy)} \times 32 \text{ (Azimuth)} \times 16 \text{ (Elevation)} = 16,384$$

Slow:

$$32 \text{ (Energy)} \times 16 \text{ (Azimuth)} \times 16 \text{ (Elevation)} = 8192$$

Hot Plasma Composition Analyzer (HPCA) [Young et al., 2016]

各衛星1基

Energy range: ~1 eV–40 keV (64 energy bins)

※FPI-DISよりやや広い

M/ΔM: 4

(H⁺, He⁺⁺, He⁺, O⁺⁺, O⁺を観測)

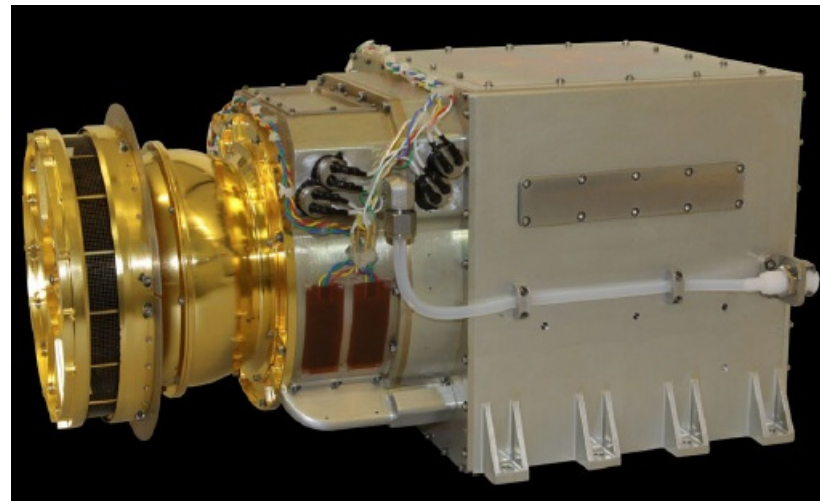
時間分解能: 10 sec (1/2 spin)

視野: 11.25° × 360°

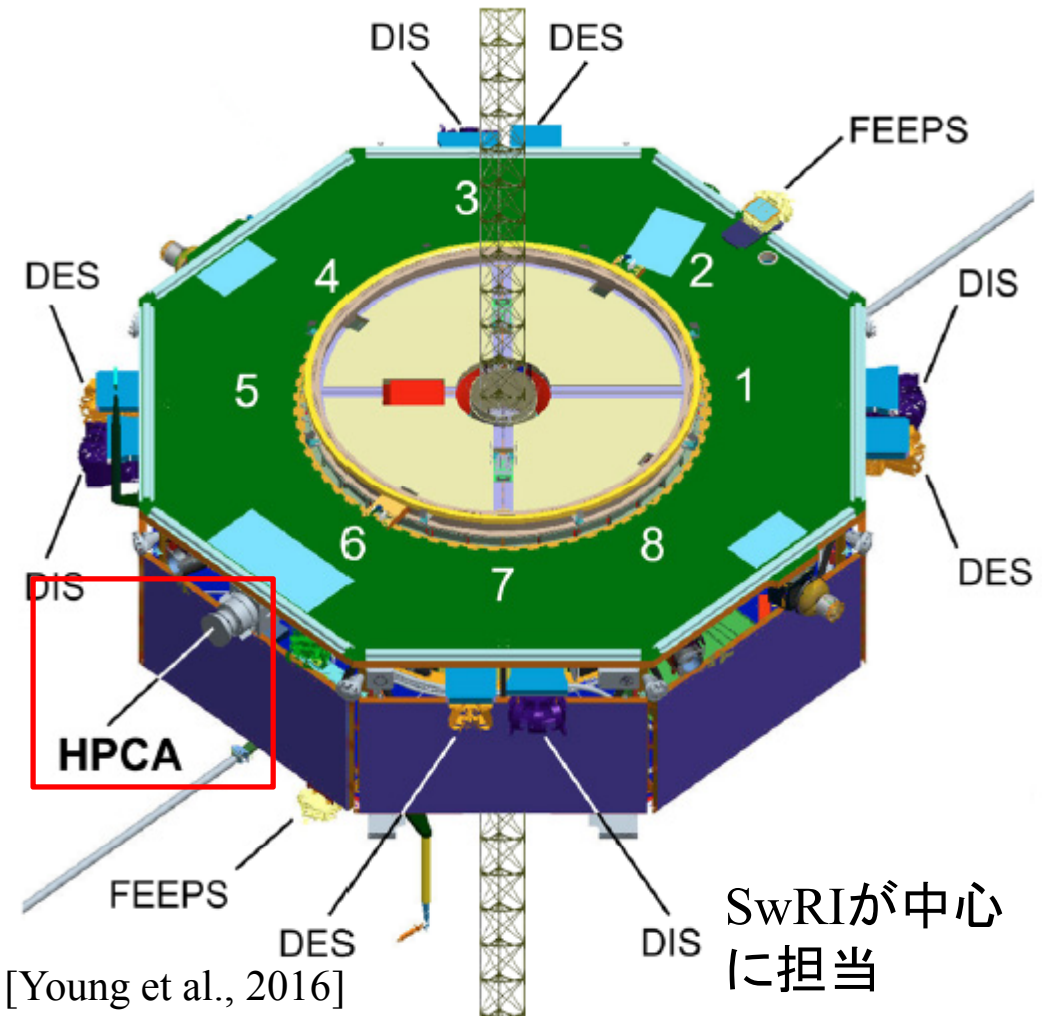
11.25° (Azimuth) × 22.5° (Elevation)

(FWHM)

16 (Azimuth) × 16 (Elevation) pixels



Slow surveyでは3.5スピン(~70 sec)のうち0.5スピンのみ計測(3.5スピンより少ない間隔の期間もあり)



Hot Plasma Composition Analyzer (HPCA) [Young et al., 2016]

各衛星1基

Energy range: ~1 eV–40 keV (64 energy bins)

※FPI-DISよりやや広い

M/ΔM: 4

(H^+ , He^{++} , He^+ , O^{++} , O^+ を観測)

時間分解能: 10 sec (1/2 spin)

視野: $11.25^\circ \times 360^\circ$

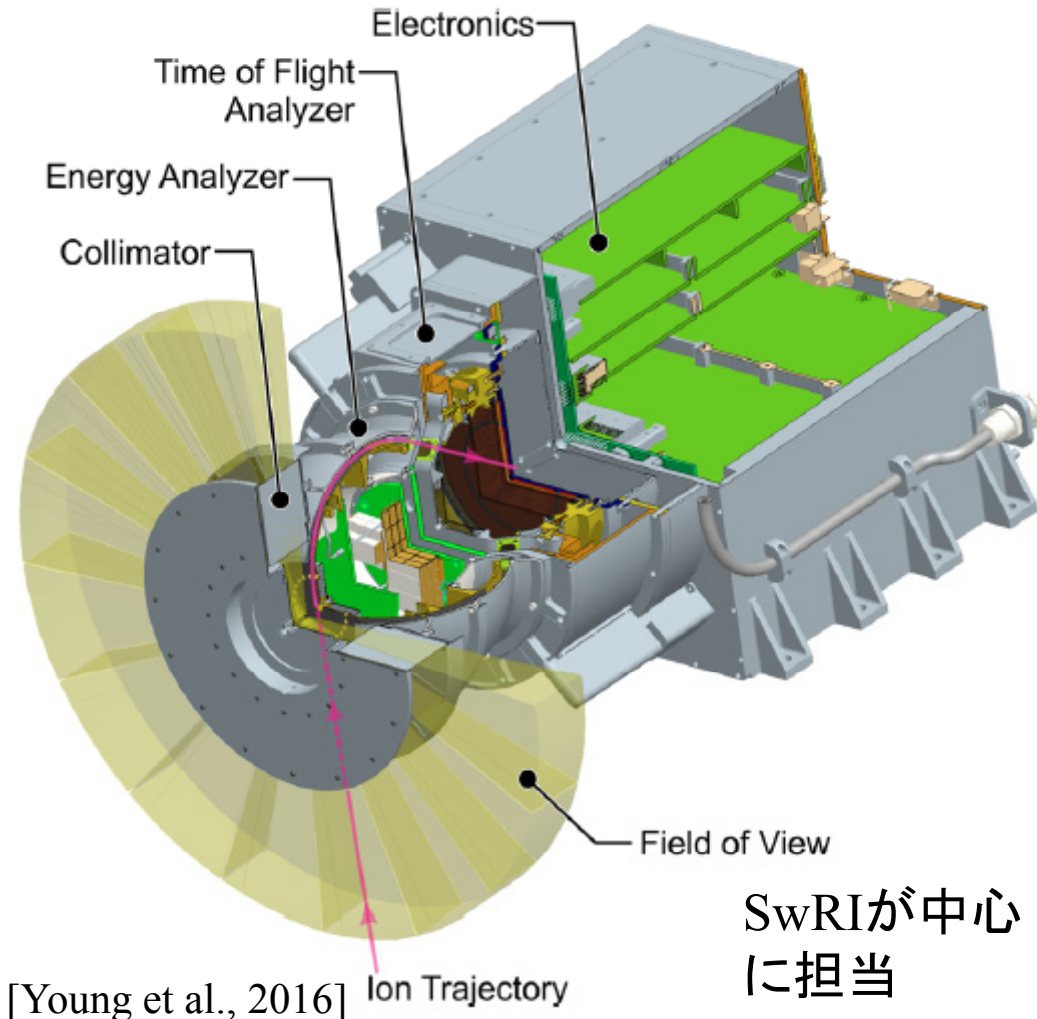
11.25° (Azimuth) $\times 22.5^\circ$ (Elevation)

(FWHM)

16 (Azimuth) \times 16 (Elevation) pixels

Fast, slow surveyではenergy binを16に、角度方向のbinを8 (Azimuth) \times 8 (Elevation)に足し合わせてダウンリンクし、元の $64 \times 16 \times 16$ の位相空間に再分配してLevel-2データとして提供 (データの配列の要素数としてはburstと変わらない)

Slow surveyでは3.5スピン(~70 sec)のうち0.5スピンのみ計測(3.5スピンより少ない間隔の期間もあり)



Hot Plasma Composition Analyzer (HPCA) [Young et al., 2016]

各衛星1基

Energy range: ~1 eV–40 keV (64 energy bins)

※FPI-DISよりやや広い

M/ΔM: 4

(H^+ , He^{++} , He^+ , O^{++} , O^+ を観測)

時間分解能: 10 sec (1/2 spin)

視野: $11.25^\circ \times 360^\circ$

11.25° (Azimuth) $\times 22.5^\circ$ (Elevation)

(FWHM)

16 (Azimuth) \times 16 (Elevation) pixels

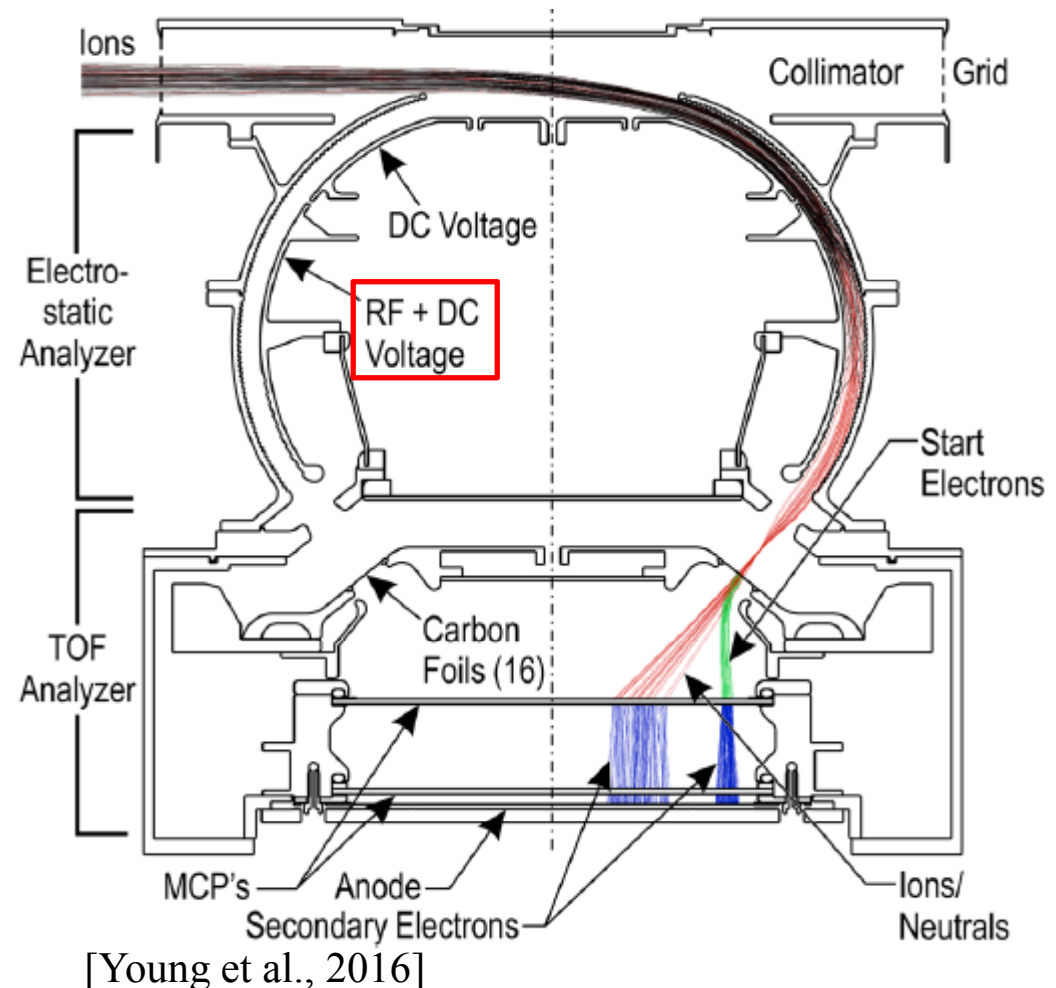
シースで大フラックスの H^+ が受かってしまう

500 eV–4 keV (14 energy bins)において、交流をかけて H^+ のフラックスを100分の1以下に抑える事ができる機能を搭載(Fast Survey中)

→ダイナミックレンジの増加($>10^5$)

→ O^+ への混入の大幅低減

Slow surveyでは3.5スピン(~70 sec)のうち0.5スピンのみ計測(3.5スピンより少ない間隔の期間もあり)



Energetic Particle Detector (EPD)

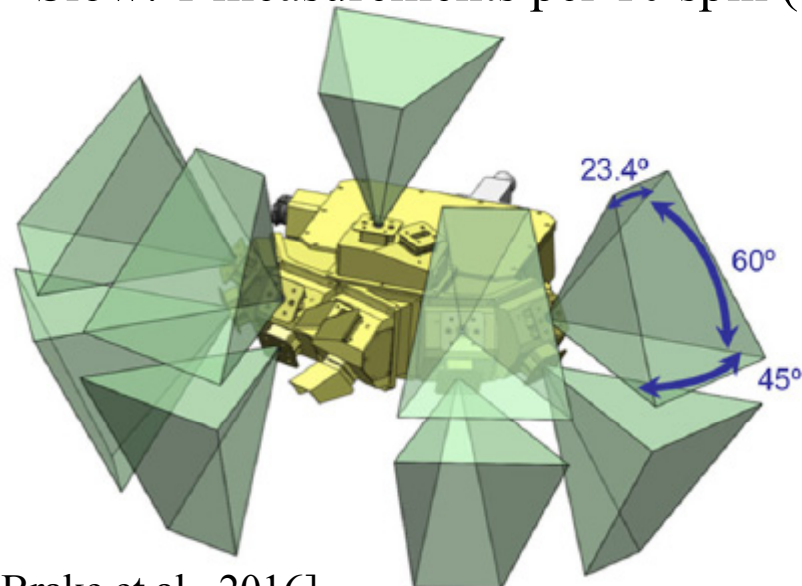
Fly's Eye Energetic Particle Spectrometer (FEEPS) [Blake et al., 2016]

Electron: 25–550 keV (15 energy channels), >550 keV (1 channel)

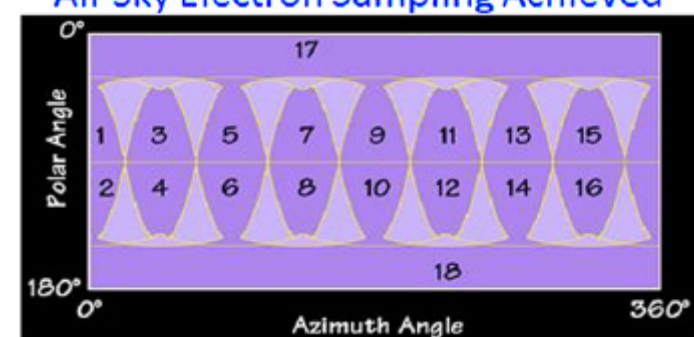
Burst: 64 measurements per spin (~20 sec) (~0.3125 s) (9 eyes × 2)

Fast: 8 measurements per spin (~20 sec) (~2.5 s) (5 eyes × 2)

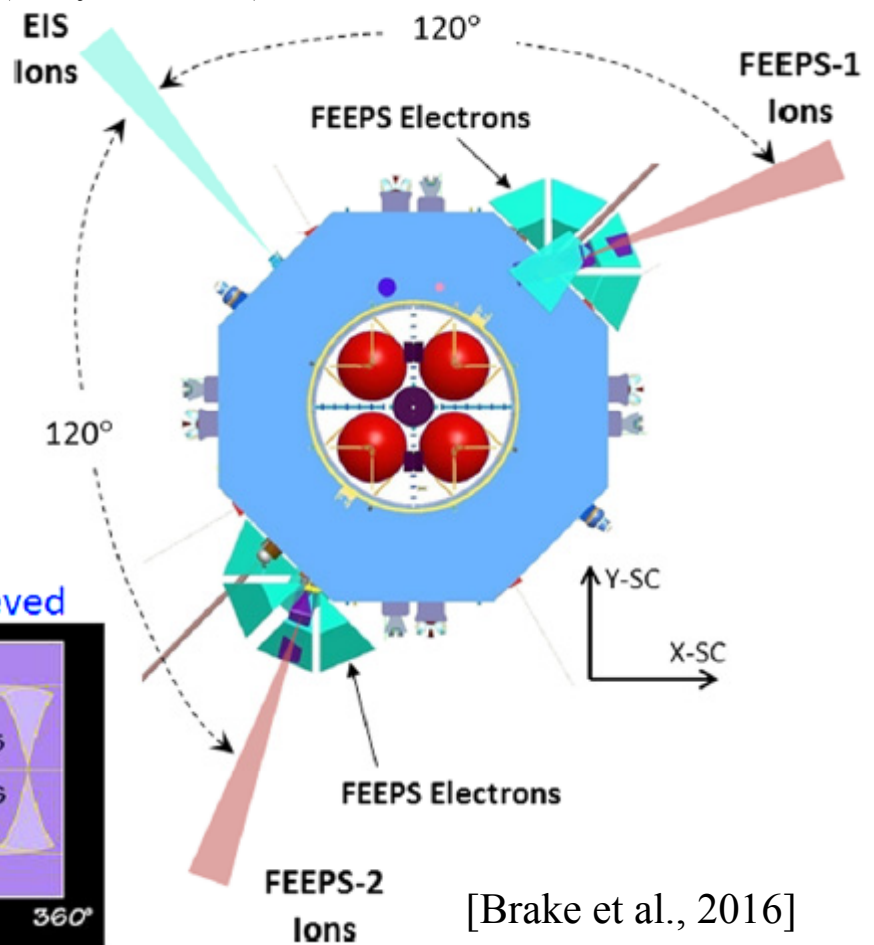
Slow: 1 measurements per 10 spin (~200 sec) (5 eyes × 2)



[Brake et al., 2016]



[Mauk et al., 2016]



[Brake et al., 2016]

◆Particle

Energetic Particle Detector (EPD)

Fly's Eye Energetic Particle Spectrometer (FEEPS) [Blake et al., 2016]

Ion: 50–600 keV (15 energy channels), >600 keV (1 channel)

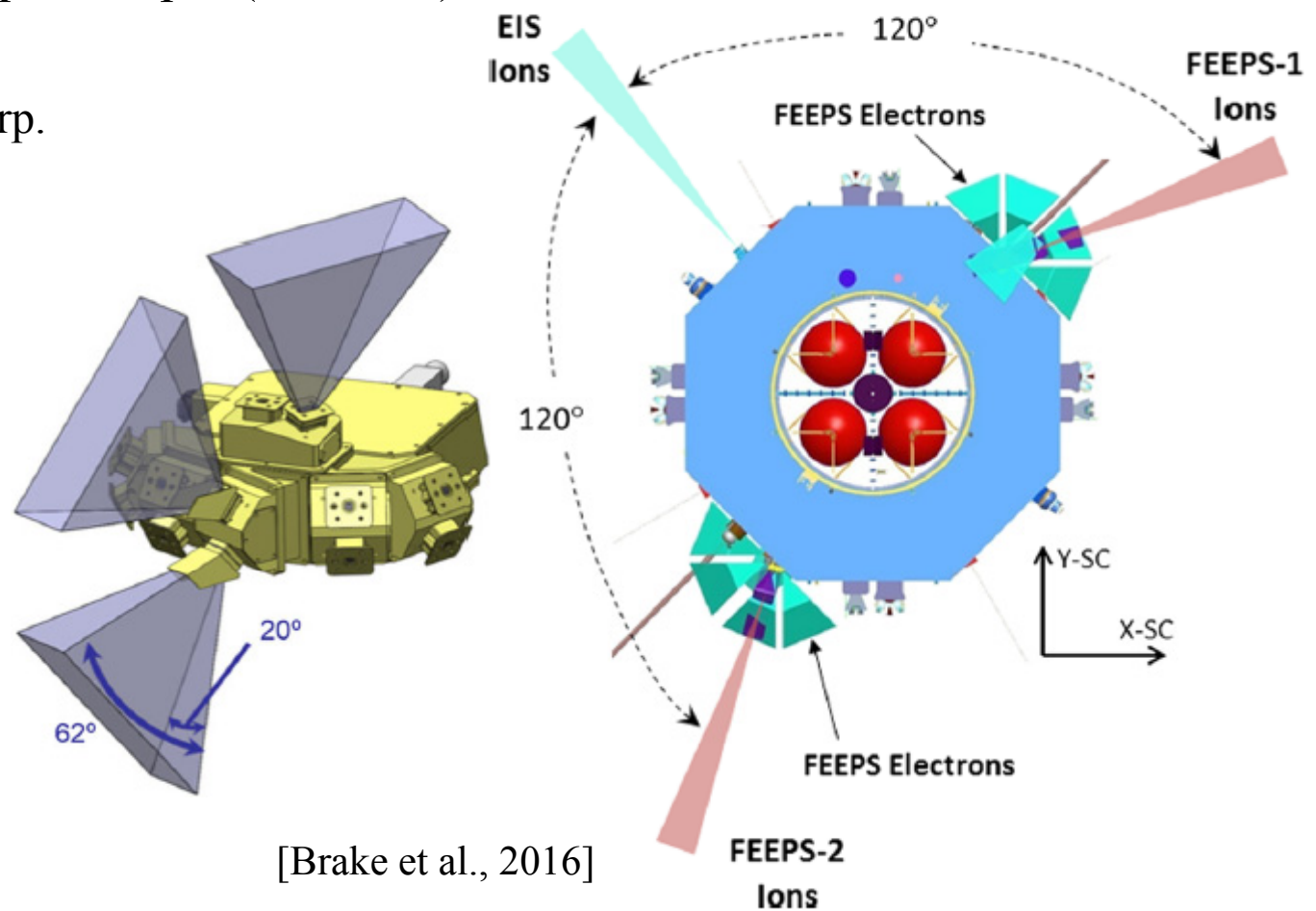
Burst: 64 measurements per spin (~20 sec) (~0.3125 s) (3 eyes × 2)

Fast: 8 measurements per spin (~20 sec) (~2.5 s) (3 eyes × 2)

Slow: 1 measurements per 10 spin (~200 sec)

FEEPSはAero Space Corp.
とLASPが中心に担当

太陽光の入射を
防ぐためスピン面
付近は計測しない



◆Particle

Energetic Particle Detector (EPD)

Energetic Ion Spectrometer (EIS) [Mauk et al., 2016]

Proton: 10–680 keV (>45 keV(TOF))

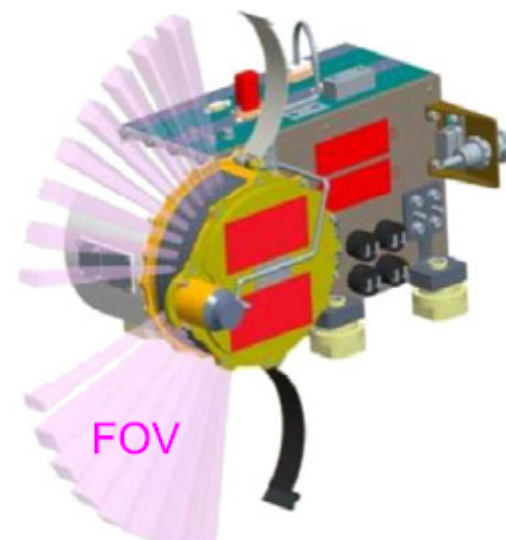
Helium or alpha: 60–960 keV (TOF only)

Oxygen: 45–1200 keV (>130 keV(TOF))

Ion (FEEPS): 45–500 keV

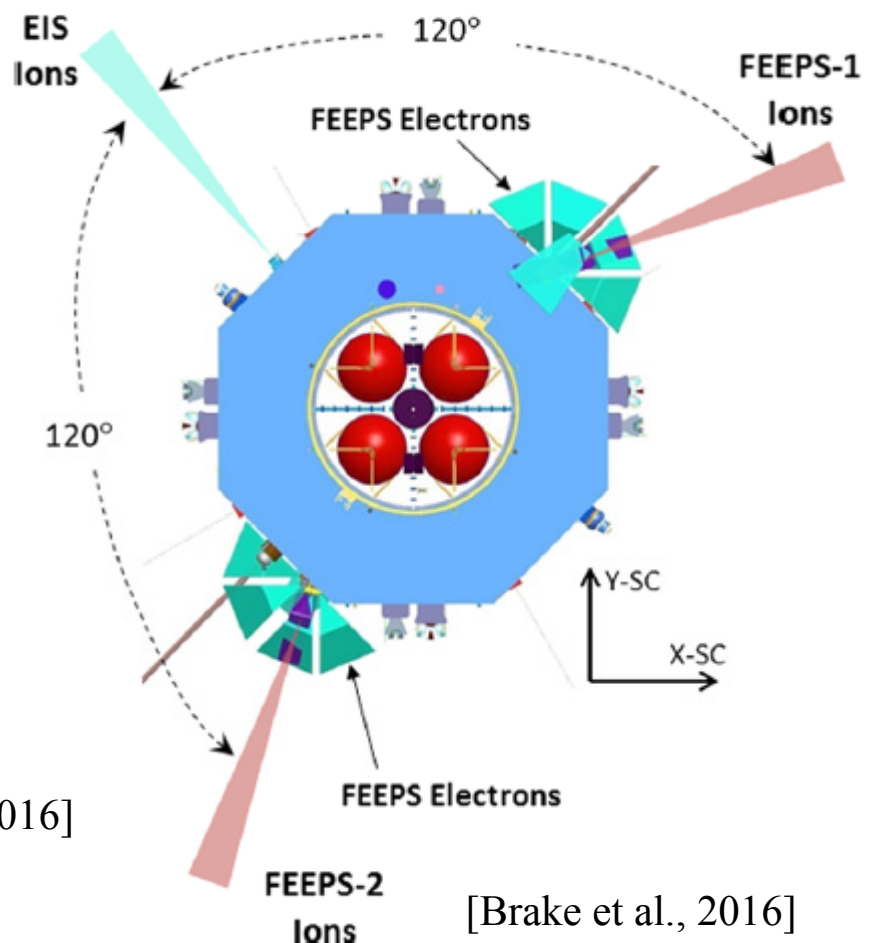
Electron: ~30–1200 keV

6 Sectors for electrons and ions



太陽光の入射を
防ぐためスピン面
付近は計測しない

[Mauk et al., 2016]



[Brake et al., 2016]

EISはJHU/APLが中心に担当
JUNOのJEDIを元に設計

VAPsのRBSPICE、New
HorizonsのPEPPSIと類似

◆ Particle

Energetic Particle Detector (EPD)

Energetic Ion Spectrometer (EIS) [Mauk et al., 2016]

Proton: 10–680 keV (>45 keV(TOF))

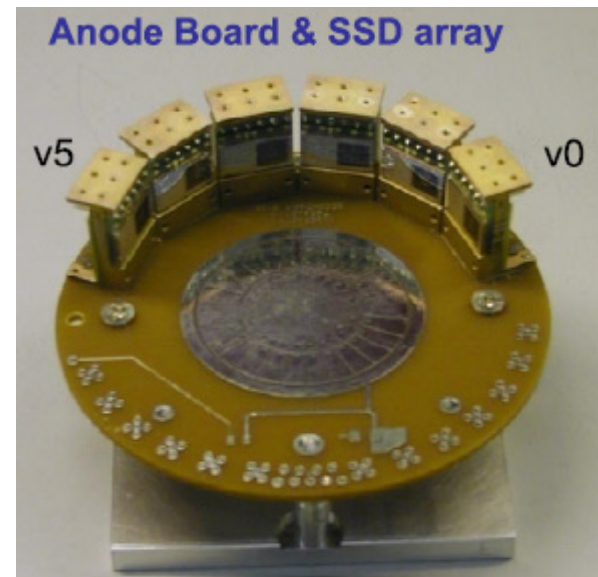
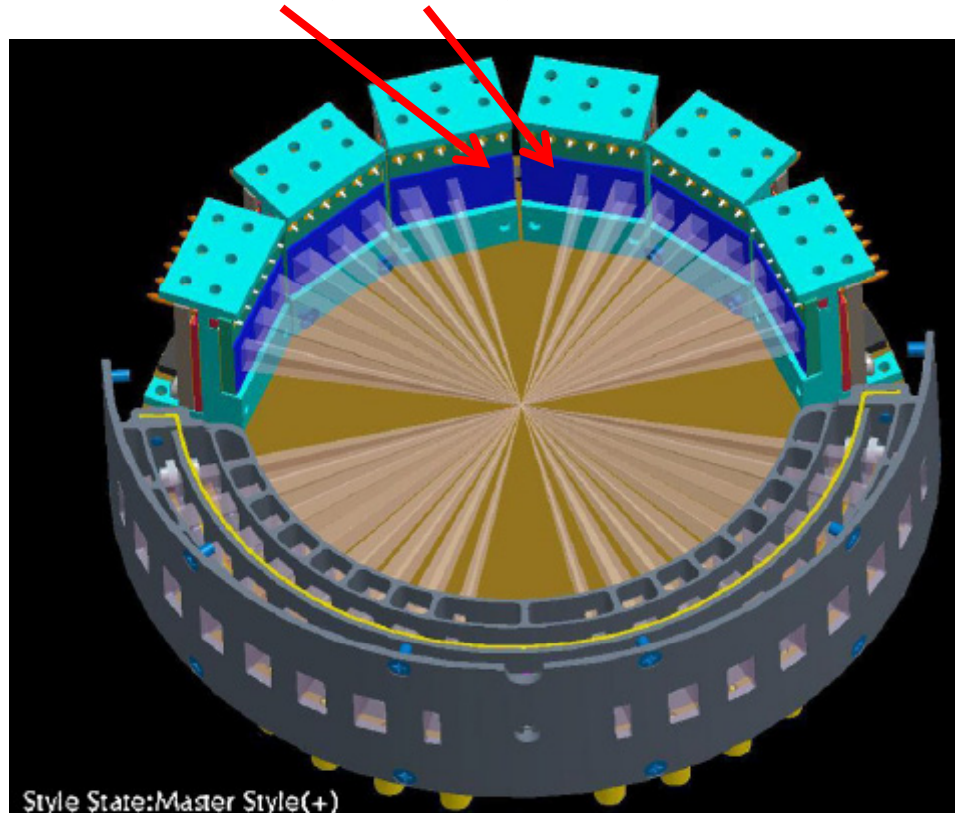
Helium or alpha: 60–960 keV (TOF only)

Oxygen: 45–1200 keV (>130 keV(TOF))

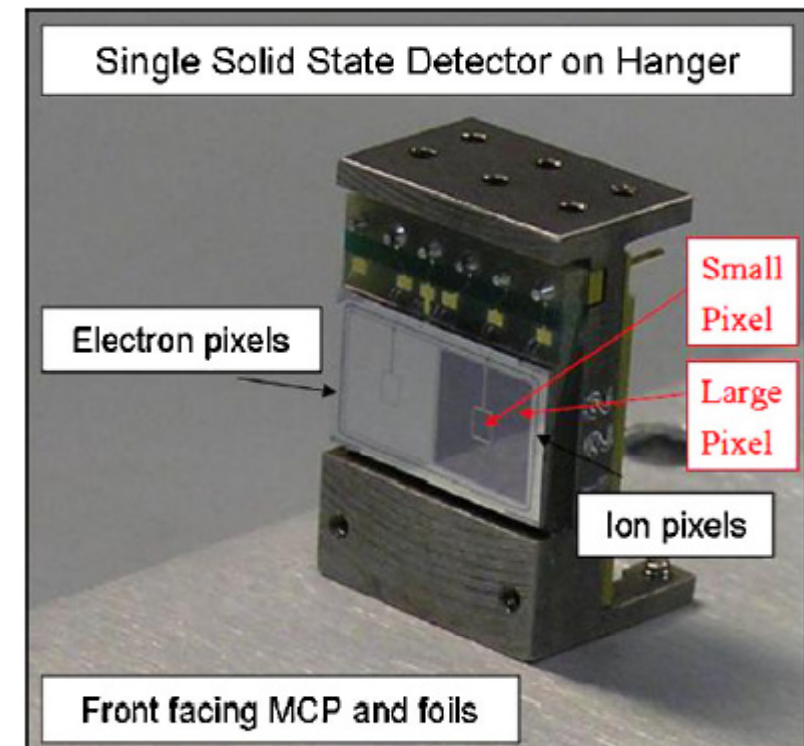
Electron: ~30–1200 keV

6 Sectors for electrons and ions

One of the ion (electron) sectors is almost masked.



43



[Mauk et al., 2016]

Energetic Particle Detector (EPD)

Energetic Ion Spectrometer (EIS) [Mauk et al., 2016]

Proton (PH): 10–80 keV (5 energy channels)

Proton (TOF): 45–680 keV (6 energy channels)

Helium (TOF): 60–960 keV (4 energy channels)

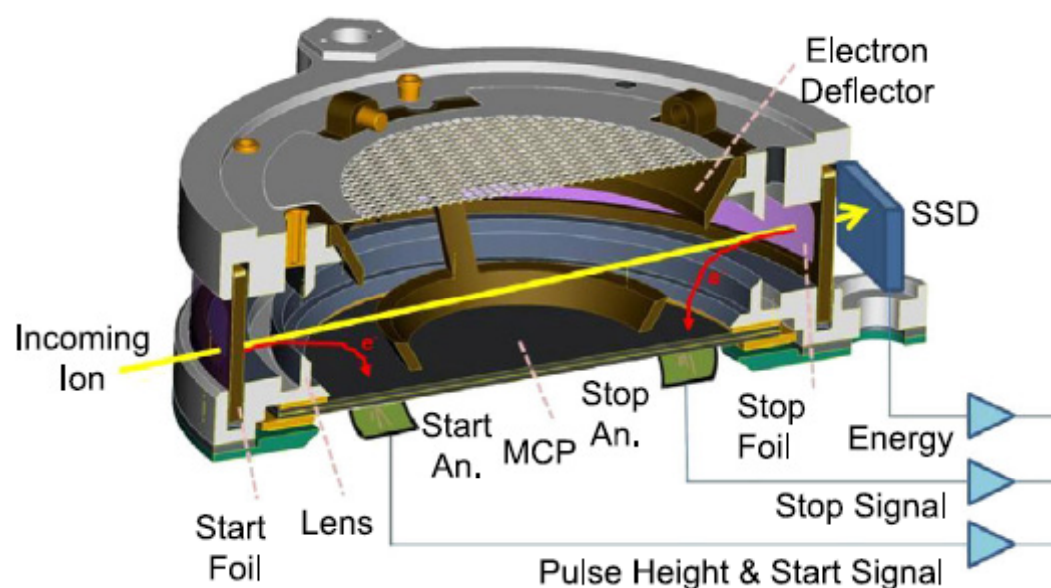
Oxygen (PH): 45–170 keV (3 energy channels)

Oxygen (TOF): 130–1200 keV (7 energy channels)

Ion (FEEPS): 45–500 keV (16 energy channels)

Electron: ~30–1200 keV (5 energy channels)

6 Sectors for electrons and ions

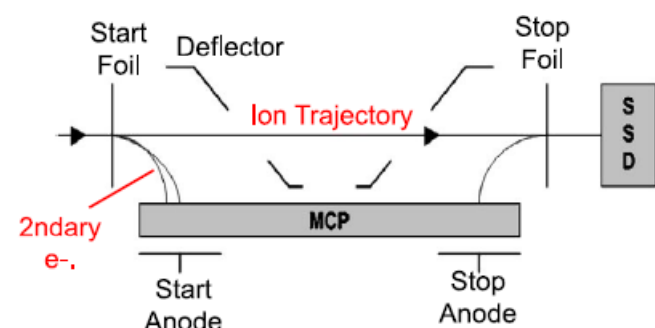


[Mauk et al., 2016]

Burst: 32 measurements per spin (~20 sec) (~0.625 s)

Fast: 8 measurements per spin (~20 sec) (~2.5 s)

Slow: 1 measurements per 10 spin (~200 sec)



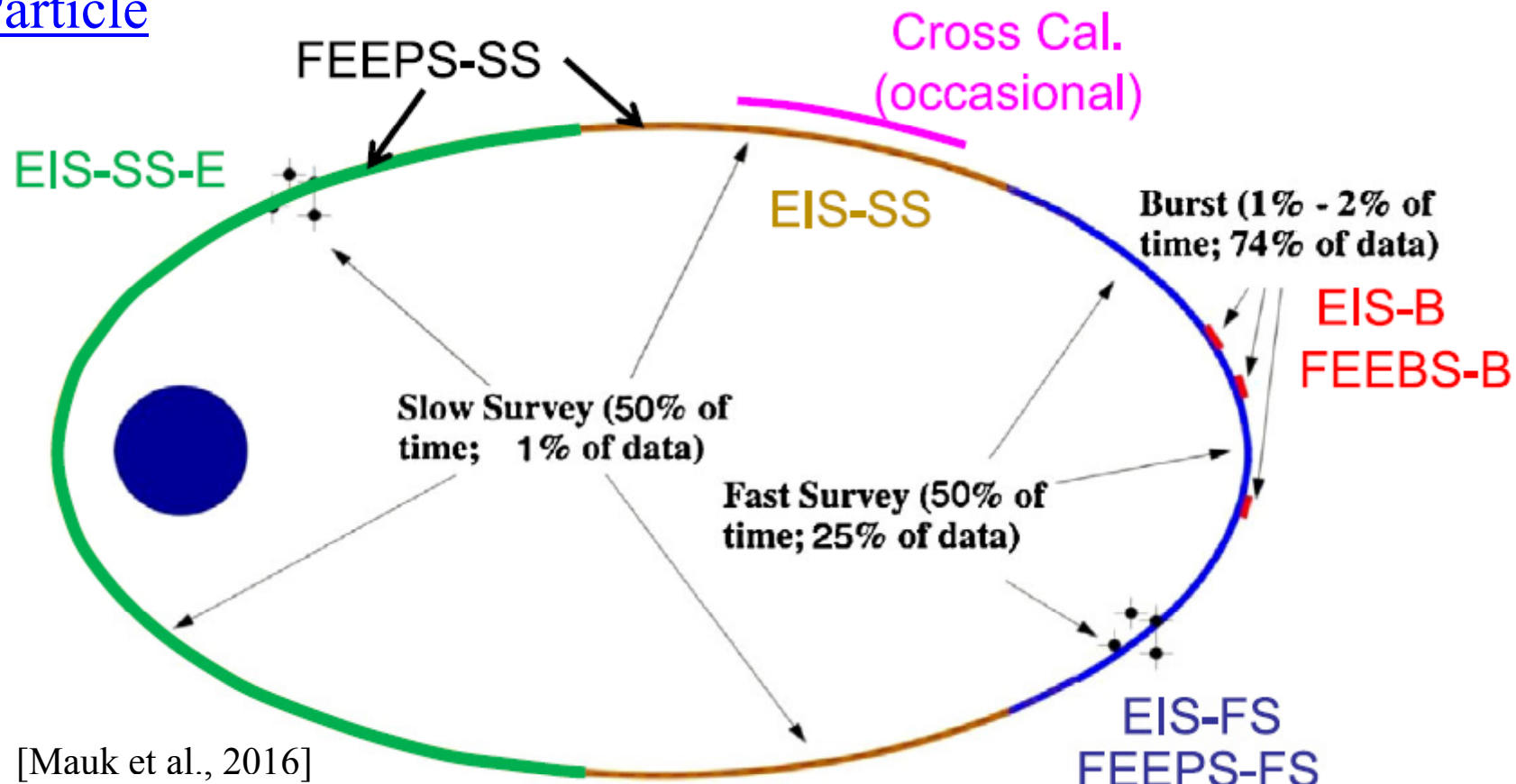
[Brake et al., 2016]

Energetic Particle Detector (EPD)Fly's Eye Energetic Particle Spectrometer (FEEPS) [Blake et al., 2016]

- 打ち上げ時に粒子入射部分のフォイルが多数破損したため、衛星の位相によって検出器に太陽光が当たってしまい、カウントが出ててしまっている
→SPEDASでのburst dataロード時には各検出器で太陽光の影響が含まれてしまう位相のデータはマスクできるようにしてある
- Phase-1aのsurvey dataは太陽光の影響がある可能性があり、注意が必要
MMS1が最も破損の影響が少なく、MMS2はMMS1よりわずかに影響大
MMS3はMMS1, 2よりも広い位相で使用不可で、MMS4が最も深刻
- 電子の一部の検出器で70 keV未満の2つのエネルギーBINの値に異常がある
(フラックスが小さい)ケースが存在

Energetic Ion Spectrometer (EIS) [Mauk et al., 2016]

- MMS1のイオン組成データはFebruary 4, 2016以降無い(January 21, 2016以降不調)
- MMS1の電子検出センサー(6 sector)のうち1つが不調
- 電子はFEEPSでも計測しているので、伝送データ量の節約のため、2週間交代で2機ずつデータを取得



少なくともPhase-2終了まではFPI, HPCA, EIS, FEEPS-Ionは放射線帯付近では計測を行わない

→FEEPS-Electron: 25–>650 keV(時間分解能: ~200秒)のみ

※電磁場のデータ(~8 samples/s)、波動のスペクトル(16秒平均)は内部磁気圏であってもある程度は使えるはず

Phase-1xで長時間日陰のある期間(June 12–July 28, 2016)は粒子計測器全ての観測を中断

◆お知らせ等

MMS全観測機器のデータ公開: 原則取得後30日でLevel-2を公開
(HPCAはやや処理が遅れている)

SPEDASで全機器のデータの解析が可能

各機器の詳細な説明や解析の注意点等は、

<https://lasp.colorado.edu/mms/sdc/public/datasets/>
で入手可能

位置等の情報: <https://lasp.colorado.edu/mms/sdc/public/> (MMS Science Data Center)
※現在約24時間周期のため、どのあたりにいるかの見当がつけやすい

- Conjunction Event Finder (<http://ergsc.isee.nagoya-u.ac.jp/cef/cef.cgi>)にMMSの軌道データとサマリープロットを追加
- ミッションの概要、観測機器等の論文がSpace Science Reviews特集号に掲載
- Science、GRL特集号に初期成果の論文出版

質問、相談等は、北村(kitamura@stp.isas.jaxa.jp)まで

◆参考文献(MMS特集号)

- Baker, D. N., et al. (2016), Magnetospheric multiscale instrument suite operations and data system, *Space Sci. Rev.*, **199**, 545–575, doi:10.1007/s11214-014-0128-5.
- Blake, J. B., et al. (2016), The Fly's Eye Energetic Particle Spectrometer (FEEPS) sensors for the Magnetospheric Multiscale (MMS) mission, *Space Sci. Rev.*, **199**, 309–329, doi:10.1007/s11214-015-0163-x.
- Burch, J. L., et al. (2016), Magnetospheric multiscale overview and science objectives, *Space Sci. Rev.*, **199**, 5–21, doi:10.1007/s11214-015-0164-9.
- Ergun R. E., et al. (2016), The axial double probe and fields signal processing for the MMS mission, *Space Sci. Rev.*, *Space Sci. Rev.*, **199**, 167–188, doi:10.1007/s11214-014-0115-x.
- Fuselier, S. A., et al. (2016), Magnetospheric multiscale science mission profile and operations, *Space Sci. Rev.*, **199**, 77–103, doi:10.1007/s11214-014-0087-x.
- Le Contel, O., et al. (2016), The search-coil magnetometer for MMS, *Space Sci. Rev.*, **199**, 257–282, doi:10.1007/s11214-014-0096-9.
- Lindqvist, P.-A., et al. (2016), The spin-plane double probe electric field instrument for MMS, *Space Sci. Rev.*, **199**, 137–165, doi:10.1007/s11214-014-0116-9.
- Mauk, B. H., et al. (2016), The Energetic Particle Detector (EPD) Investigation and the Energetic Ion Spectrometer (EIS) for the Magnetospheric Multiscale (MMS) mission, *Space Sci. Rev.*, **199**, 471–514, doi:10.1007/s11214-014-0055-5.
- Pollock, C. J., et al. (2016), Fast plasma instrument for MMS, *Space Sci. Rev.*, **199**, 331–406, doi:10.1007/s11214-016-0245-4.
- Russell, C. T., et al. (2016), The magnetospheric multiscale magnetometers, *Space Sci. Rev.*, **199**, 189–256, doi:10.1007/s11214-014-0057-3.
- Torbert, R. B., et al. (2016a), The FIELDS Instrument Suite on MMS: Scientific objectives, measurements, and data products, *Space Sci. Rev.*, **199**, 105–135, doi:10.1007/s11214-014-0109-8.
- Torbert, R. B., et al. (2016b), The Electron Drift Instrument for MMS, *Space Sci. Rev.*, **199**, 283–305, doi:10.1007/s11214-015-0182-7.
- Torkar, K., et al. (2016), Active spacecraft potential control investigation, *Space Sci. Rev.*, **199**, 514–544, doi:10.1007/s11214-014-0049-3.
- Young, D.T., et al. (2016), Hot plasma composition analyzer for the Magnetospheric Multiscale Mission, *Space Sci. Rev.*, **199**, 407–470, doi:10.1007/s11214-014-0119-6.

Table 1 DFG specifications

| | |
|---|--|
| Board size | $7 \times 11 \text{ cm}^2$ |
| Board mass | 76 g |
| Supply voltages | 3.3 V (digital), 8 V (analogue) |
| Power consumption | 450 mW (nominal) |
| Digital resolution | 24 bits |
| Dynamic range | $\pm 650 \text{ nT}$ (low range) $\pm 10,500 \text{ nT}$ (high range) |
| Noise density at 1 Hz | $< 8 \text{ pT}/\sqrt{\text{Hz}}$ (low range) $< 100 \text{ pT}/\sqrt{\text{Hz}}$ (high range) |
| Offset drift with electronics temperature | $< 5 \text{ pT}/^\circ\text{C}$ (low range) $< 10 \text{ pT}/^\circ\text{C}$ (high range) |
| Offset drift with sensor temperature | $< 10 \text{ pT}/^\circ\text{C}$ (both ranges) |
| Gain drift with electronics temperature | $< 10 \text{ ppm}/^\circ\text{C}$ (low range) $< 15 \text{ ppm}/^\circ\text{C}$ (high range) |
| Gain drift with sensor temperature | $< 60 \text{ ppm}/^\circ\text{C}$ (low range) $< 350 \text{ ppm}/^\circ\text{C}$ (high range) |
| Non-linearity | $< 3 \times 10^{-5}$ (low range) $< 6 \times 10^{-4}$ (high range) |

Table 2 Specifications of the Analogue Fluxgate Magnetometer

| | | |
|---------------------|--|--------------------------------------|
| Board Size | $23.2 \times 19.1 \text{ cm}$ | |
| Board Mass | 285 grams | |
| Power Consumption | 1.2 W | |
| Dynamic Range | High: $\pm 8200 \text{ nT}$ | Low: $\pm 510 \text{ nT}$ |
| Noise Levels @ 1 Hz | High: $10 \text{ pT}/\sqrt{\text{Hz}}$ | Low: $5 \text{ pT}/\sqrt{\text{Hz}}$ |
| Nyquist Frequency | 64 Hz | |

[Russell et al., 2016]

◆ FIELDS

Table 9 In-flight calibration methods

| Calibrated item | Comparator | Method | Frequency |
|---------------------------|-------------------------------|--|---|
| AFG/DFG orthogonality | None | Spin plane quadrature, Spin-tone removal | Every orbit |
| AFG/DFG gains and offsets | Observatory AFG/DFG | Inter-observatory comparison | Monthly, or as needed |
| AFG/DFG gains | Spin-plane reference phase | Perigee pass analysis | Initial, quarterly or higher phase 1, 2 |
| FG offsets | None | Variance analysis, Solar Wind | Yearly, as available |
| FG spin-axis offsets | EDI | Direction, TOF comparison | Weekly |
| SCM gains | AFG, DFG | Overlapping frequency band | Monthly |
| SCM gains, phase, offsets | None | Waveform analysis of cal signals | Daily |
| SDP, ADP gains | AFG, DFG | $-\mathbf{V}_{sc} \times \mathbf{B}$ perigee comparison | Initial, monthly phase 1, 2 |
| SDP, ADP gains | FPI, HPCA | Solar Wind $-\mathbf{V} \times \mathbf{B}$ comparison | As available |
| SDP, ADP gains, offsets | EDI | Direct \mathbf{E}_{perp} comparison | Continual, distinguishing different plasma regimes |
| SDP, ADP offsets | DFG, AFG | $\mathbf{E} \cdot \mathbf{B} = 0$ check | Quiet regions |
| SDP, ADP offsets | HPCA | $-\mathbf{V}_{O+} \times \mathbf{B}$ comparison | Lobe outflow regions |
| EDI MCP gains | None | Ambient response: MCP, pre-amp | Monthly |

[Torbert et al., 2016a]

Table 1 Summary of SDP instrument characteristics

| | |
|---|---------------------------------------|
| Total mass per unit | 4.30 kg |
| Total power per unit (secondary) | 380 mW |
| Boom cable length | 57 m (nominal deployed length) |
| Boom cable diameter | 1.55 mm |
| Boom cable density | 5.06 g/m |
| Boom cable surface material | Silver-plated braid |
| Preamplifier dimensions | 31 mm diameter × 71 mm length |
| Preamplifier mass | 86 g |
| Preamplifier surface material | DAG213 coated aluminium |
| Thin wire length | 1.75 m (nominal deployed length) |
| Thin wire diameter | 0.24 mm |
| Thin wire density | 0.155 g/m |
| Thin wire surface material | Titanium |
| Probe diameter | 80 mm |
| Probe mass | 93 g (47 g sphere, 46 g yoyo) |
| Probe surface material | Titanium nitride |
| Probe 1, 2, 3, 4 direction in X-Y plane | 30, 210, 120, 300 degrees from X-axis |
| Radial distance to hinge point | 1.6 m |
| Probe–probe distance | 120.92 m (nominal) |
| Bias current range | [−550, +110] nA |
| Outer guard range | [−10, +10] V relative to probe |
| Inner guard range | [−10, +10] V relative to probe |
| Electric field measurement range | ±500 mV/m |
| Electric field measurement resolution | 0.05 mV/m |
| Electric field measurement accuracy | 0.3 mV/m |
| Electric field frequency range | DC to 100 kHz |

[Lindqvist et al., 2016]

Table 3 Gains, ranges and sensitivities of ADP, SDP, and SCM signals

| Signal(s) | Antenna length ¹ | | DSP gain ² | DC – 100 Hz | | | AC: At ~ 5 kHz | | |
|-----------------|-----------------------------|-----------|-----------------------|-------------|----------------------|--------------------|--------------------------|----------------------|--------------------|
| | Physical | Effective | | Preamp gain | Amplitude Resolution | Range ³ | Preamp gain ⁴ | Amplitude Resolution | Range ⁵ |
| V1–V4 | 60 m | 48 m | 0.0208 | 1.00 | 3.7 mV | –100–30 V | 0.85 | 4.4 mV | ±14.7 V |
| V5, V6 | 15.1 m | 7.3 m | 0.0208 | 1.00 | 3.7 mV | –100–30 V | 0.8 | 4.6 mV | ±15.6 V |
| V1ac; V2ac | 60 m | 48 m | 0.1991 | – | – | – | 0.85 | 9.4 µV/m | ±306 mV/m |
| E12; E34 | 120 m | 96 m | 0.0415 | 1.00 | 19 µV/m | ±626 mV/m | 0.85 | 22 µV/m | ±306 mV/m |
| E56 | 30.4 m | 14.5 m | 0.211 | 1.00 | 25 µV/m | ±817 mV/m | 0.8 | 31 µV/m | ±1.02 V/m |
| E12ac; E34ac | 120 m | 96 m | 0.0996 | – | – | – | 0.85 | 9.3 µV/m | ±306 mV/m |
| E56ac | 30.4 m | 14.5 m | 0.1991 | – | – | – | 0.8 | 33 µV/m | ±1.08 V/m |

[Ergun et al., 2016]

Table 8 FIELDS routine data products

| Sensor (s) | Description |
|------------------------------|--|
| FIELDS Quicklook products | |
| AFG | 3-component B-field from Analog Flux Gate (AFG), to 16 vectors/s |
| DFG | 3-component B-field from Digital Flux Gate (DFG), to 16 vectors/s |
| SDP-ADP | 3-component E-field from Spin-plane Double Probe (SDP) and Axial Double Probe (ADP), to 32 samples/s |
| SDP-ADP | 3-component Low Frequency (LF) electric spectra, 1–8000 Hz |
| SDP-ADP | 3 sampled Medium Frequency (MF) electric spectra, 25–100 kHz |
| SCM | 3-component LF magnetic spectra, 2–6000 Hz |
| EDI | Ambient electrons at two directions |
| FIELDS Level 2 products | |
| AFG | 3-component B-field from Analog Flux Gate (AFG), to 128 vectors/s |
| DFG | 3-component B-field from Digital Flux Gate (DFG), to 128 vectors/s |
| SDP-ADP | 3-component E-field from Spin-plane Double Probe (SDP) and Axial Double Probe (ADP), to 8192 samples/s |
| SDP-ADP | 3-component AC E-field from Spin-plane Double Probe (SDP) and Axial Double Probe (ADP), to 8192 samples/s |
| SDP-ADP | 3-component high speed burst E-field from Spin-plane Double Probe (SDP) and Axial Double Probe (ADP), to 65536 samples/s |
| SDP-ADP | 1 spacecraft potential sample from combination of ADP and SDP |
| SDP-ADP | 3 sphere voltages from ADP and SDP |
| SDP-ADP | 3-component Low Frequency (LF) electric spectra, 1–8000 Hz |
| SDP-ADP | 3 sampled Medium Frequency (MF) electric spectra, 25–100 kHz |
| SCM | 3-component AC B-field waveform from Search Coil Magnetometer (SCM) |
| SCM | 3-component high speed AC B-field waveform, to 16384 samples/s |
| SCM | 3-component LF magnetic spectra, 2–6000 Hz |
| EDI | Electric fields and drift velocity from Electron Drift Instrument (EDI) |
| EDI | Ambient electrons at two directions |
| FIELDS Level 2-plus products | |
| AFG-DFG-SCM | 3-component combined B-field from all Mag sensors, to 1024 or greater vectors/s |
| SDP-ADP-EDI | 3-component E-field from Spin-plane Double Probe (SDP) and Axial Double Probe (ADP) and Electron Drift Instrument (EDI), to 8192 samples/s |

[Torbert et al., 2016a]

Table 2 HPCA performance requirements

| Parameter | Variable | Required Value |
|---------------|-----------------------------------|--|
| Sensitivity | Energy-dependent geometric factor | $3 \times 10^{-3} \text{ cm}^2 \text{ sr keV/keV}$ (total) |
| | Maximum potential counting rate | 20 MHz |
| Mass/charge | Range | 1 to 16 amu/e |
| | Resolution ($M/\Delta M$) | 4 at FWHM |
| Energy/charge | Range | 10 eV to 40 keV |
| | Resolution ($\Delta E/E$) | ≤ 0.2 FWFM |
| | Energy range scan rate | 64 log-spaced samples per 0.625 s |
| Angle | Field-of-regard | $11.25^\circ \times 360^\circ$ |
| | Field-of-view resolution | 11.25° azimuth $\times 22.5^\circ$ elevation FWFM |
| | Number of pixels over 4π sr | 32 azimuth \times 16 elevation |
| Dynamic range | Maximum detectable energy flux | $\sim 3 \times 10^9 \text{ keV/cm}^2 \text{ sr s keV}$ of H ⁺ |
| | Minimum detectable energy flux | $\sim 3 \times 10^4 \text{ keV/cm}^2 \text{ sr s keV}$ of H ⁺ |
| | Dynamic range | $\gtrsim 10^5$ |
| Timing | 3-D velocity distribution | $\frac{1}{2}$ spacecraft spin (10 s) |
| | 2-D energy-elevation scan | 625 ms |
| | Single sample all elevations | 8.95 ms |

[Young et al., 2016]

The FIELDS Instrument Suite on MMS

Table 2 Nominal modes of FIELDS CEB

| Quantity | Type | Components | Samples/s | | | |
|----------|-------------|------------|-------------|-------------|---------------|---------------|
| | | | Slow survey | Fast survey | Burst-phase 1 | Burst-phase 2 |
| EDI | Coded | Beam pair | ~16 | ~16 | ~125 | ~125 |
| AFG | Time series | 3 | 8 | 16 | 128 | 128 |
| DFG | Time series | 3 | 8 | 16 | 128 | 128 |
| DC-E | Time series | 3 | 8 | 32 | 1024 | 8192 |
| AC-E | Time series | 3 | | | 8192 | 8192 |
| DC-V | Time series | 1 to 3 | 8 | 32 | 1024 | 8192 |
| SCM | Time series | 3 | 8 | 32 | 1024 | 8192 |
| LFE | Spectra | 1 or 3 | 0.0625 | 0.5 | | |
| MFE | Spectra | 1 or 3 | 0.0625 | 0.5 | | |
| LFB | Spectra | 1 or 3 | 0.0625 | 0.5 | | |
| HSB-E | Time series | 3 | | | 65536@40 % | 65536@10 % |
| HSB-B | Time series | 3 | | | 16384@40 % | 16484@10 % |

LFE (1–8000 Hz)

[Torbert et al., 2016a]

MFE (25 Hz–100 kHz)

LFB (2–6000 Hz)

Table 1 DES and DIS performance requirements and measured performance

| Parameter | Requirement | Measured performance |
|-------------------------------------|---|---|
| Dual Electron Spectrometers (DES) | | |
| Instantaneous polar FOV | 180° | 180° |
| Polar angle resolution | ≤ 15° | 9–15° |
| Azimuth separation | 45° ± 0.5° | 45° ± 0.5° |
| Azimuth FOV deflection | Up to ±17° | > ±17° |
| Azimuth FOV width | ≤ 11.25 | 4–11° |
| Energy/charge range | 0.01–30 keV | 0.01–30 keV |
| Energy/charge width | ≤ 20 % | 14–20 % |
| Pixel geometric factor | ≥ 1 × 10 ⁻⁴ cm ² sr eV/eV | (1–7) × 10 ⁻⁴ cm ² sr eV/eV |
| 3D time resolution | 30 ms | 30 ms (coarser at 7.5 ms) |
| Sample integration time | 195 μs | 195 μs |
| Avg. HV settling time ¹ | ≤ 39 μs (EOL) | 24–27 μs (BOL) |
| Total HV settling time ¹ | ≤ 5 ms (EOL) | 3.1–3.4 ms (BOL) |
| Dual Ion Spectrometers (DIS) | | |
| Instantaneous polar FOV | 180° | 180° |
| Polar angle resolution | ≤ 15° | ≤ 15° |
| Azimuth separation | 45° ± 0.5° | 45° ± 0.5° |
| Azimuth FOV deflection | Up to ±17° | > ±17° |
| Azimuth FOV width | ≤ 11.25 | 4–6.5° |
| Energy/charge range | 0.01–30 keV | 0.01–30 keV |
| Energy/charge width | ≤ 20 % | 11–15 % |
| Pixel geometric factor | ≥ 5 × 10 ⁻⁴ cm ² sr eV/eV | 1–2 × 10 ⁻⁴ cm ² sr eV/eV |
| 3D time resolution | 150 ms | 150 ms (coarser at 37.5 ms) |
| Sample integration time | 1 ms | 1 ms |

¹BOL = Beginning of Life; EOL = End of Life.

[Pollock et al., 2016]